NAME [redacted]

DATE 05-09-2013

UNIVERSITY OF OKLAHOMA

GRADUATE COLLEGE

STRATIGRAPHY AND PALYNOMORPHS COMPOSITION OF THE WOODFORD SHALE IN THE WYCHE FARM SHALE PIT, PONTOTOC COUNTY, OKLAHOMA

A THESIS

SUBMITTED TO THE GRADUATE FACULTY

in partial fulfillment of the requirements for the

Degree of

MASTER OF SCIENCE

By

CARLOS EDUARDO MOLINARES BLANCO
Norman, Oklahoma
2013

STRATIGRAPHY AND PALYNOMORPHS COMPOSITION OF THE WOODFORD SHALE IN THE WYCHE FARM SHALE PIT, PONTOTOC COUNTY, OKLAHOMA

A THESIS APPROVED FOR THE
CONOCOPHILLIPS SCHOOL OF GEOLOGY AND GEOPHYSICS

BY

[redacted]

Dr. Roger Slatt, Chair

[redacted]

Dr. Paul Philp

[redacted]

Mr. Brian Cardott

A Liliana y Camila, por su constante paciencia, apoyo e infinita fuente de inspiración...A mis padres, hermanos y a mi abuelita por todo su amor...

To Liliana and Camila, because of their continuous patience, support and infinite source of inspirations...To my parents, brothers and grandma for all their love...

Acknowledgements

I would like to give my first special thanks to Dr. Roger Slatt, who provided me all the data and resources for this project. Dr Slatt's supervision, advise, technical guidance, patience and support gave me the opportunity to learn all that I know now about the fascinating world of the unconventional oil and gas shales.

I would like to express my gratitude to Dr. Paul Philp and Brian Cardott, for their reviews and all the time they put into serving on my thesis committee. I really appreciate that Brian shared with me valuable information about the Woodford Shale which significantly helped to improve this research.

I am very grateful to Devon Energy Corporation and Schlumberger, who generously provided the Wyche-1 well data set to the Institute of Reservoir Characterization. Richard Traver from the Oklahoma Petroleum Information Center (OPIC) granted me the well log files for the regional correlation. Rick Andrews and Neil Suneson (OGS) offered their constructive discussion and help during my data gathering process.

I thank the University of Oklahoma and principally the faculty staff and professor from the ConocoPhillips School of Geology and Geophysics. Dr. Slatt, Dr. Marfurt, Dr Mitra, Dr. Abousleimann, their lectures and practical exercises helped me to learn new concepts and master skills for this thesis.

A number of individuals have provided analytical support and data sets for this thesis: Younane N. Abousleiman, Nicole Buckner, Andrea Miceli-Romero, Paul Philp, Rafael Sierra and Minh Tran. Thank you for sharing with me your research results and ideas.

I am also grateful with my Venezuelan ("panas") and Colombian ("parseros") friends in Norman. Many ideas have been developed by talks with them, thanks a lot.

I feel immense pleasure in expressing my gratitude to Ecopetrol S.A. and ICETEX, for the generous leave of absence and the fellowship-credit awarded to me during my graduate studies.

The last but not least, to my daughter Cami Molinares and to my wife Lili Leon, for their inspiration, support, patience and stolen time during the course of this research.

Table of Contents

List of Tables

List of Figures

Abstract

This work presents a detailed lithofacies description and sequence stratigraphy model for the fine grained rocks cored at the Wyche-1 well, in the Lawrence Uplift, Pontotoc County, Oklahoma.

The detailed core description, thin sections, XRD mineralogy, geochemical analysis and wire-line log data have led to the identification of nine lithofacies: siliceous laminate and finely laminated mudstones (lithofacies A and B), and calcareous mudstones (lithofacies C) are associated with the Mississippian "Pre-Welden Shale" at 0 to 24 m (0-80 ft); argillaceous mudstones with phosphate and pyritic nodules (lithofacies D and E), are generally identified within the upper Woodford interval at 24 to 37 m (80-122 ft). The organically richest shales (lithofacies F1 and F2) are associated with the middle Woodford at 37 to 53 m (122-174 ft); and siliceous/argillaceous mudstone with thin clay laminations (lithofacies G) and argillaceous siltstone with abundant angular detrital quartz (lithofacies H) are commonly related to the lower Woodford at 53 to 65 m (174-212 ft).

The Woodford Shale in the Wyche-1 well is present between two unconformities which are associated with 2nd order sequence stratigraphy boundaries. The highest Gamma Ray (GR) log values and organically richest deposits in the middle Woodford comprise a 2nd order Condensed Section (CS), limited at the top by a maximum flooding surface (*mfs*). The GR log transgressive and regressive patterns, the palynological assemblages (Pollen Index) and the Ti/Al and Si/Al ratios illustrate that the lower and middle Woodford correspond to 2nd order Transgressive System Tract

(TST) deposits and the upper Woodford to 2nd order Highstand System Tract (HST) deposits.

The lithofacies stacking patterns in the Woodford and "Pre Welden" Shales recognized during the detailed core lithofacies description were coupled with GR log variations and grouped into 3rd order cycles. These cycles are bounded by marine-flooding surfaces, characterized by high GR values (kick) and turnaround points of the lithostratigraphic stacking patterns.

The lower and middle Woodford contain together five 3rd order cycles and the upper Woodford contains six 3rd order cycles. The 3rd order cycles were also subdivided into ductile, organic-rich transgressive hemicycles and brittle, quartz-rich regressive hemicycles. The hypothetical best brittle intervals for "fracking" are related to middle Woodford 3rd order regressive hemicycles, characterized by a high biogenic quartz content, high acoustic (P-wave) impedances, high anisotropy, high Young's modulus and low Poisson's ratio.

Finally, this work also suggests that erosion and paleogeography features during the early Mississippian, possibly affected the Woodford Shale thickness and the distribution of the Woodford play in the Arkoma Basin. The Woodford Shale is thicker toward the southwest, but this trend is interrupted in the center of the basin, where the Mississippian sequence overlying the Woodford Shale is thicker and where the Misener-Woodford sequence unconformably truncates the underlying Sylvan Shale and older units.

1. Introduction

The Woodford Shale, Late Devonian - Early Mississippian in age, is considered one of the most important unconventional gas and oil shale resources in North America (Cardott, 2012). The Woodford is considered as a excellent hydrocarbon source rock, with high total organic carbon content and Type II kerogen (Miceli-Romero and Philp, 2012). It is also fracturable due to intervals rich in biogenic quartz, derived primarily from radiolarian and sponge spicules (Kirkland et al., 1992).

The Woodford has been tested as a potential hydrocarbon producer since as early as the 1950's. However, production started to increase in 2004 when gas production increased from only ~0.4 billion cubic feet (Bcf) and ~1.500 barrels of oil (bbl) in January to more than 27 Bcf and ~ 140,000 bbl of oil during January 2010 (Grieser, 2011). Principally, the production increments were associated with four major areas: (1) Anadarko Basin; (2) Cherokee Platform; (3) Southern Oklahoma Ardmore Basin and (4) Arkoma Basin (Cardott, 2012).

Particularly in the Arkoma Basin, well designs, brittleness, permeability, matrix porosity and magnitude of natural fracturing has a large effect on hydrocarbon production (Andrews, 2009). The stratigraphic controls behind these variables tend to be minimized and even ignored, partly because of the difficulty in identifying stratigraphic patterns from fine-grained rocks (Slatt et al., 2012).

However, the basic concepts of sequence stratigraphy are now commonly applied to organic-rich, fine grained rocks (e.g. Singh, 2008; Abouelresh and Slatt, 2012; Rodriguez and Slatt, 2012; Slatt et al., 2012). These concepts coupled with

geomechanic properties (Slatt and Abousleiman, 2011) make brittle intervals readily mappable and may facilitate identifying ductile-brittle couplets during exploration and exploitation activities.

In an effort to better understand the rock properties of the Woodford Shale in the western portion of the Arkoma Basin, the University of Oklahoma, Devon Energy Corporation and Schlumberger teamed up to core and log the Woodford Shale section behind an active shale pit quarry in Pontotoc County, south central Oklahoma (Slatt et al., 2012). As part of this attempt, the principal objectives in this thesis work were:

(1) to develop a detailed lithofacies description from the Wyche-1 Core; (2) to build a 3rd Order Sequence Stratigraphy model base on the Gamma Ray (GR) log; (3) to compare the cycles interpreted from the GR log, with the palynological assemblages and Si/Al and Ti/Al ratios, in order to confirm the transgressive and regressive cycles interpreted; (4) to explore possible paleogeographic controls on the distribution of the Woodford Shale thickness in the Arkoma Basin.

2. Previous Works

2.1 Regional Setting

The Arkoma Basin is an east-west trending basin in eastern Oklahoma. It is approximately 40 miles (~65 km) wide by 260 miles (~420 km) long, and covers approximately 13,000 square miles (20.900 km^2) (Figure 1a).

The Arkoma Basin is limited southward by the Ouachita Mountains, northward by the Cherokee Platform and the Ozark Uplift, and westward by the Arbuckle Mountains (Johnson and Cardott 1992). The Choctaw thrust fault system defines the southern basin edge with the Ouachita Mountains. It is characterized by complex thrusted pre-Pennsylvanian units, often yielding repeat sections and detachment faults related to the Woodford Shale (e.g. Suneson et al., 2005; 2009). The Arkoma Basin limit toward the north is associated with sediment truncation toward the Cherokee Platform and the Ozark Uplift (Figure 1a,b).

The Arkoma Basin was preceded by a stable continental shelf passive margin from Cambrian to Mississippian time (Johnson and Cardott, 1992; Northcutt and Campbell, 1996). During this time interval, thick and relatively shallow water sequences were deposited until the Late Mississippian, when a regional tectonic event caused a tilt toward the south and the truncation of the shelf deposits toward the north (Figure 1b). This tectonic event was related with the initial development of the Appalanchian-Ouachita belt and with the initial withdrawal of the sea during the Late Mississippian (Sutherland, 1988).

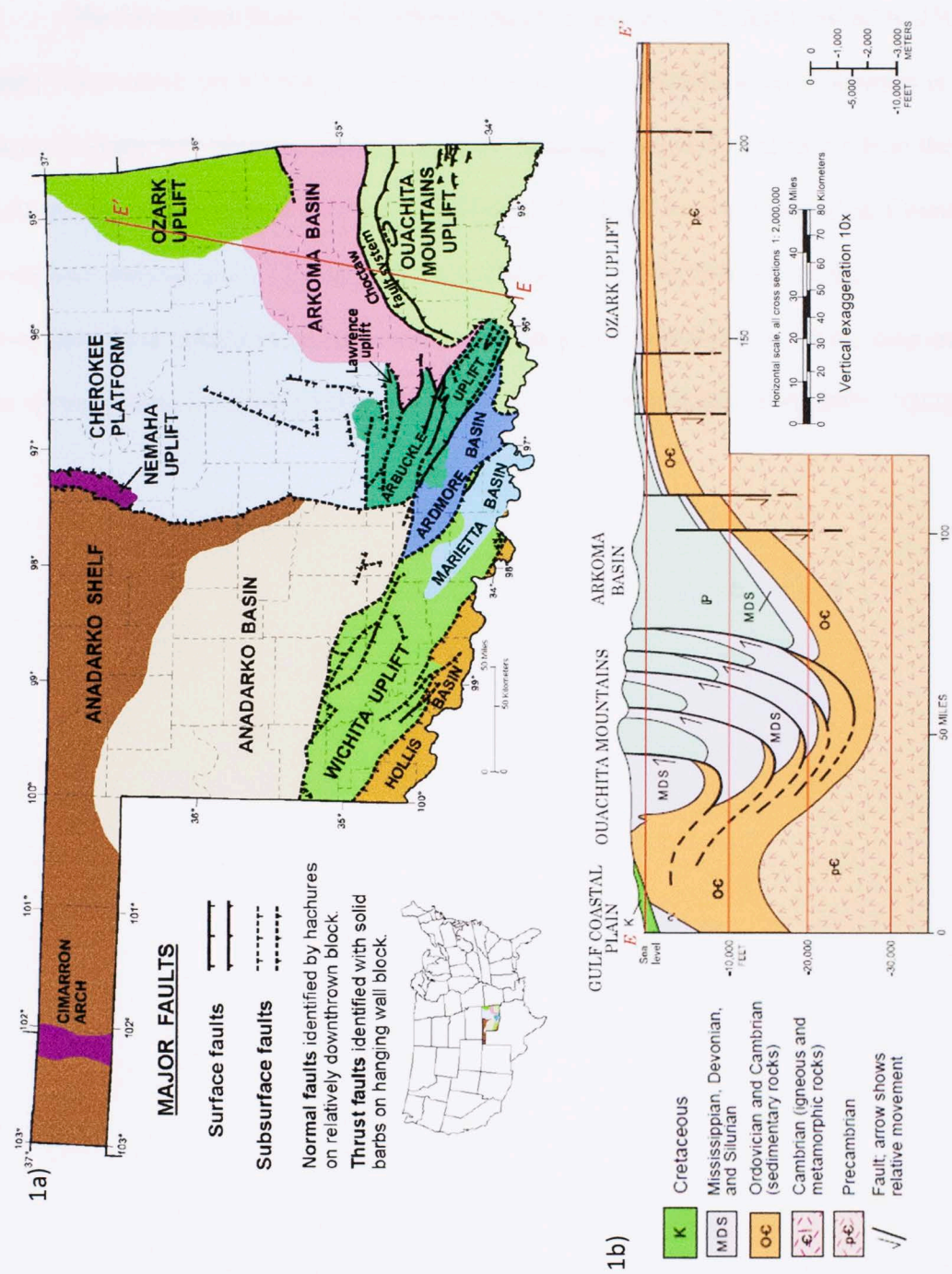

Figure 1a). Oklahoma tectonic provinces. b) Schematic cross section throughout the Ozark Uplift, Arkoma Basin and the Ouachita Mountains.
(Modified from Cardott, 2012 and Johnson, 2008)

The Woodford Shale in the Arkoma Basin is generally 100 feet (~30 m) to 250 feet (~75 m) thick but thins to < 50 feet (~15 m) in the northeast and west, where it is exposed along the Lawrence Uplift (Figure 2). Most horizontal Woodford wells in the Arkoma Basin have been drilled within a trend that extends from northern Coal County northward through much of Hughes County (Andrews, 2009). In this area, the Woodford Shale ranges from 5,000 feet (~1,500 m) to 10,500 feet (~3,200 m) deep and the vitrinite reflectance (Ro) values range from 1 to 2.5 % (Cardott 2005; 2007; 2012).

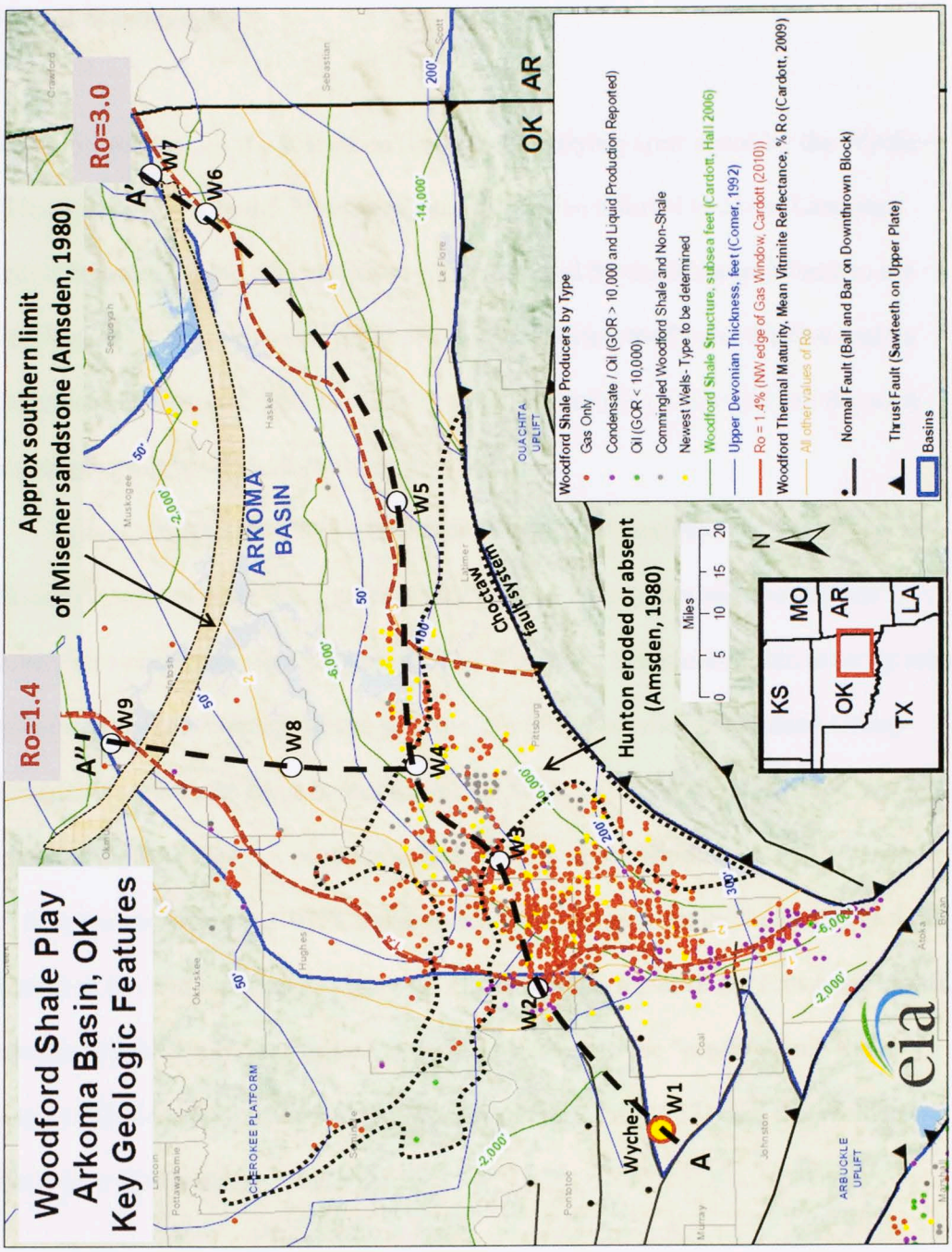

Figure 2. Woodford Shale play in the Arkoma Basin, Oklahoma.
White dots, wells used in the regional cross section A-A' and A-A". The colored dots represent horizontal and vertical wells producing from the Woodford Shale with first production from 01-01-2001 to 06-01-2011. Location of the Wyche-1 well is shown (W1).Source: http://www.eia.gov/oil_gas/rpd/shaleusa6.pdf.

2.2 Local Stratigraphy

This project focuses on the Woodford Shale and overlying units cored by the Wyche-1 well in the Lawrence Uplift. The Lawrence Uplift, also referred to as the Lawrence Horst, is bounded by the Ahloso Fault to the north and by the Stonewall Fault to the south (Figure 3). The Lawrence Uplift was formed during the Pennsylvanian and its western end was uplifted more than its eastern part, exposing older rocks to the west and younger rocks to the east (Slatt et al., 2012).

In the Lawrence Uplift, the Woodford Shale is approximately 120 feet (~40 m) thick and consists of hard, black to dark black-brown, thinly laminated shale that weathers into platy fragments (Figure 4). The Woodford Shale is overlain there by some units termed as "pre-Welden" shale, and the Woodford overlies the Hunton Group (Barrick et al., 1990). In the Arkoma Basin, the Misener Sandstone sometimes lies at the base of the Woodford. It contains conodonts which are Middle to Late Devonian in age (Amsden and Klapper, 1972), but it seems to be geographically limited toward the northeast of the Arkoma Basin (Figure 2). On the southern part of the Lawrence Uplift, where the Wyche-1 well was drilled, a shale equivalent to the "pre-Welden" shale disconformably overlies the top of the Woodford (Branson, 1957), and the Welden Limestone is absent (Over, 1992).

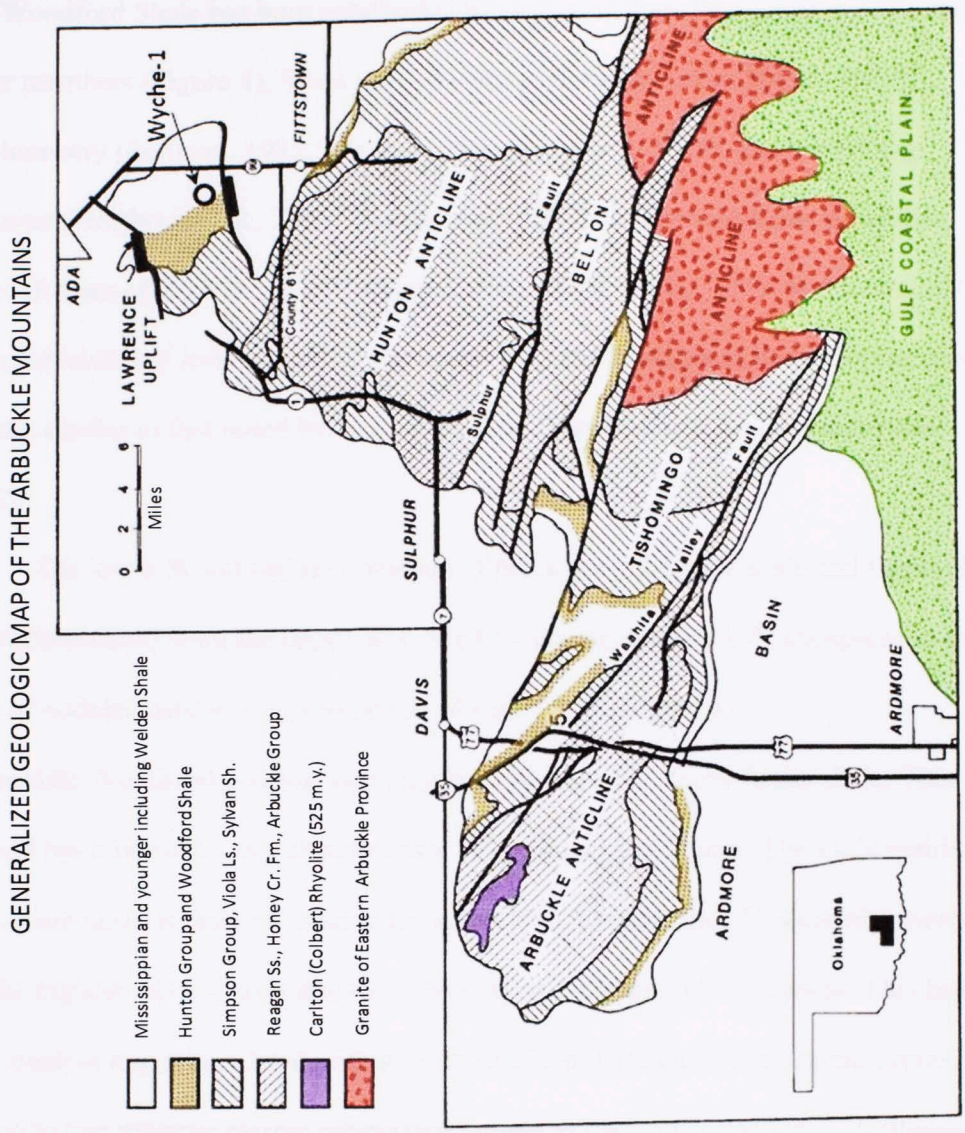

Figure 3. Generalized geologic map of the Arbuckle Mountains
The Lawrence Uplift is limited northward by the Ahloso Fault and southward by the Stonewall Fault. The Wyche-1 well was located at the base of lower Mississippian units in order to obtain the most complete Woodford Shale interval (After Ritter, 1990).

The Woodford Shale has been subdivided by several authors into lower, middle and upper members (Figure 4), based on: palynomorph distributions (Urban, 1960), geochemistry (Sullivan, 1985; Miceli-Romero and Philp, 2012), gamma ray log character (Northcutt et al., 2001; Paxton et al., 2007), and geomechanic properties (Abousleiman et al., 2007; 2009; Buckner et al., 2009; Portas, 2009; Sierra et al., 2010). The subdivision of lower, middle, and upper Woodford presented in the Wyche core is broadly similar to that noted by Slatt et al., (2012); and Miceli-Romero and Philp, (2012):

The lower Woodford is composed of black gray siliceous shale and fissile shale. It is differentiated from the upper Woodford by the apparent lack of phosphate in the form of nodules, and by the presence of silicified logs (Figure 4).

The middle Woodford is composed mainly of black to dark gray fissile shale. This interval has a frequent odor of petroleum and contains less quartz. The shale matrix is not calcareous as it does not effervesce with hydrochloride acid. This member normally has the highest gamma ray values and total organic carbon (TOC) content. This high TOC content might be related with a series of global Late Devonian anoxic events, related to two massive marine extinctions known as the Lower and Upper Kellwasser events (Walliser, 1996; McGhee, 1996) (Figure 4).

The upper Woodford is in some ways similar to the lower Woodford. It contains interbedded black to gray fissile shales and silty quartz-rich intervals, with sporadic dolomitic beds as thick as 1 foot (~0.3 m). The quartz-rich beds exhibit natural fractures perpendicular to the bedding. In some locations fractures are filled with bitumen. This

upper Woodford is differentiated from the lower by abundant phosphate lenses and pyrite and phosphate nodules, 0.5 inches (~ 1.3 cm) to > 3 feet (> 1m) in diameter.

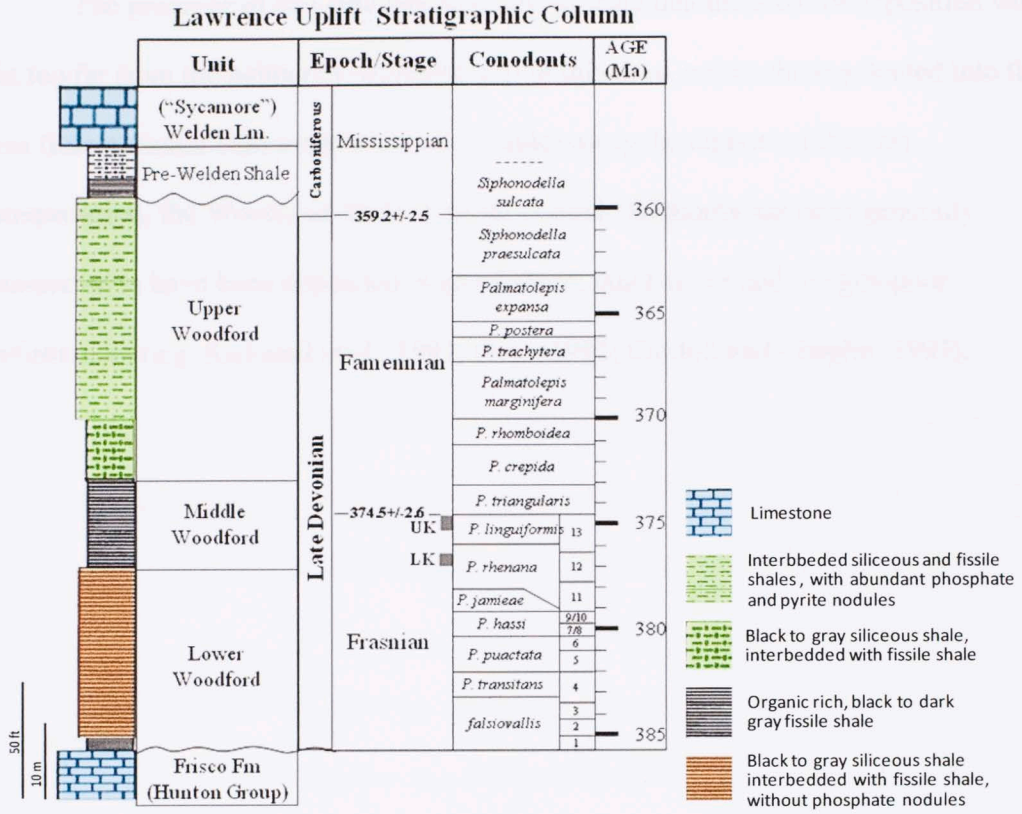

Figure 4. Lawrence Uplift stratigraphic column.
After Barrick et al., (1990); Over and Barrick, (1990); Over, (1992). The conodont zones are based on the Woodford Shale's conodont distribution at the Lawrence Uplift, reported by Over and Barrick (1990); Over (1992); Johnson and Klapper (1992). The geochronology and absolute age are after Gradstein et al (2004). UK and LK represent the approximate positions of the massive and global anoxic events known as Upper and Lower Kellwasser, respectively.

It is worth mentioning that portions of a silicified log (*Callixylon*) were found parallel to the bedding in the Wyche shale pit outcrop, lying on units corresponding to the Upper Woodford. The presence of silicified logs is common in the lower Woodford (e.g.Kirkland et al., 1992; Suneson 2010), but they have never been reported before from the upper Woodford or Mississippian in age beds. The upper Woodford has the

lowest TOC content of the three members, and it is thought to have been deposited closer to shore during a general regression (Slatt et al., 2012).

The presence of this silicified log may indicate that the locus of deposition was not too far from the habitat of *Archaeopteris* at this time, unless the log floated into the area from a distant land mass hundreds of miles away. In support of this last interpretation, the Woodford Shale in south-central Oklahoma has been generally interpreted to have been deposited in an offshore, quiet-water and oxygen-poor environment (e.g. Kirkland et al., 1992; Over, 1992; Cardott and Chaplin, 1993).

2.3 Biostratigraphy and Age Control

The Woodford Shale is Late Devonian - Lower Mississippian in age at the Lawrence Uplift (Figure 4), principally based on conodont biostratigraphy. It lies unconformably on Lower Devonian units of the Hunton Group (Amsden, 1960) and is overlain by Early Mississipian units (Over and Barrick, 1990; Over, 1992).

Over (1990) identified some conodont species diagnostic of the Late Devonian (Frasnian Stage), from two samples immediately above the basal lag bed between the Hunton Group and the Woodford Shale (Johnson and Klapper, 1992). The uppermost Woodford Shale contains a well-preserved and diverse conodont fauna which represents the Late Famennian - Early Mississippian boundary (Over and Barrick, 1990; Over, 1992).

The Late Devonian conodant fauna that occurs near the top of the Woodford Shale is characterized by *Pseudopolygnathus marburgensis trigonicus*, *Palmatolepis gracilis gracilis*, and *Pelekysgnathus guizhouensis*. The *Pseudopolygnathus marburgensis trigonicus* ranges from the Upper *P. expansa* zone through Middle *P. praesulcata* Zone (Figure 4). The *P. sulcata* Zone is the lowest Carboniferous conodont zone and it was identified at the Lawrence Uplift by the first occurrence of *Siphonodella duplicata* (Over and Barrick, 1990; Over, 1992).

The Woodford Shale age in the Wyche-1 core could not be based upon palynological analysis, since only new species with unknown stratigraphic ranges dominate the fossil assemblages. The species recovered until noware not comparable with those reported from other Devonian-Mississippian localities. In addition, the

ecological zonation schemes proposed by previous authors (Urban, 1960; Von Almen, 1970) occupy roughly similar stratigraphic positions, but they are facies-controlled, possibly non-synchronous and unknown with respect to their absolute age (Von Almen, 1970).

3. Data set

The Wyche-1 well was drilled, cored and logged about 500 feet (~150 m) east of an active quarry in the Wyche shale pit, Pontotoc County, Oklahoma (Slatt et al., 2012). This well-core was part of a multidisciplinary research project between the University of Oklahoma, Devon Energy and Schlumberger in 2006 (Figure 5).

The total core was described and analyzed at the Reservoir Characterization Institute of the University of Oklahoma, except some pieces of core which were immersed and preserved in mineral oil PG1 for additional geomechanics studies. The core recovery was 95%, which is equivalent to 180 feet (~54 m). Unfortunately, during the coring process the Woodford Shale - Hunton contact was missed by only 2 feet (~ 0.6 m). However, the contact was recorded by the Formation Micro Imager (FMI) log (Figure 6). The gamma and spectral core gamma ray logs were also provided by Devon Energy and used with the FMI® log for correlating the facies described in core with the Wyche-1 well logs (Figure 7).

A total of 12 core samples were selected for thin sections, according to intervals of interest. The thin sections were used to determine rock fabric, general mineralogical composition, cement type and fossil identification. Some thin section photos and core photos from previous descriptions were also provided. Also, 21 palynological slides were analyzed and photographed with a Zeiss AxioCam MRc5 and AxionVision Rel 4.8 software, using 10X and 20X objectives. Detailed images with an increased magnification of 40X and 65X, were also acquired for some selected palynomorphs.

The principal facies identified during the core and thin section descriptions were then characterized by Total Organic Carbon (TOC) content, Rock-Eval Analysis and X-ray diffraction (XRD) mineralogical composition. In addition, a suite of conventional Schlumberger well logs were also provided, including gamma ray, resistivity, density, neutron porosity and Element Capture Spectroscopy (ECS) log (Figure 7). All this information was used as the data set and because of the proprietary nature of data, their methods are not discussed in detail.

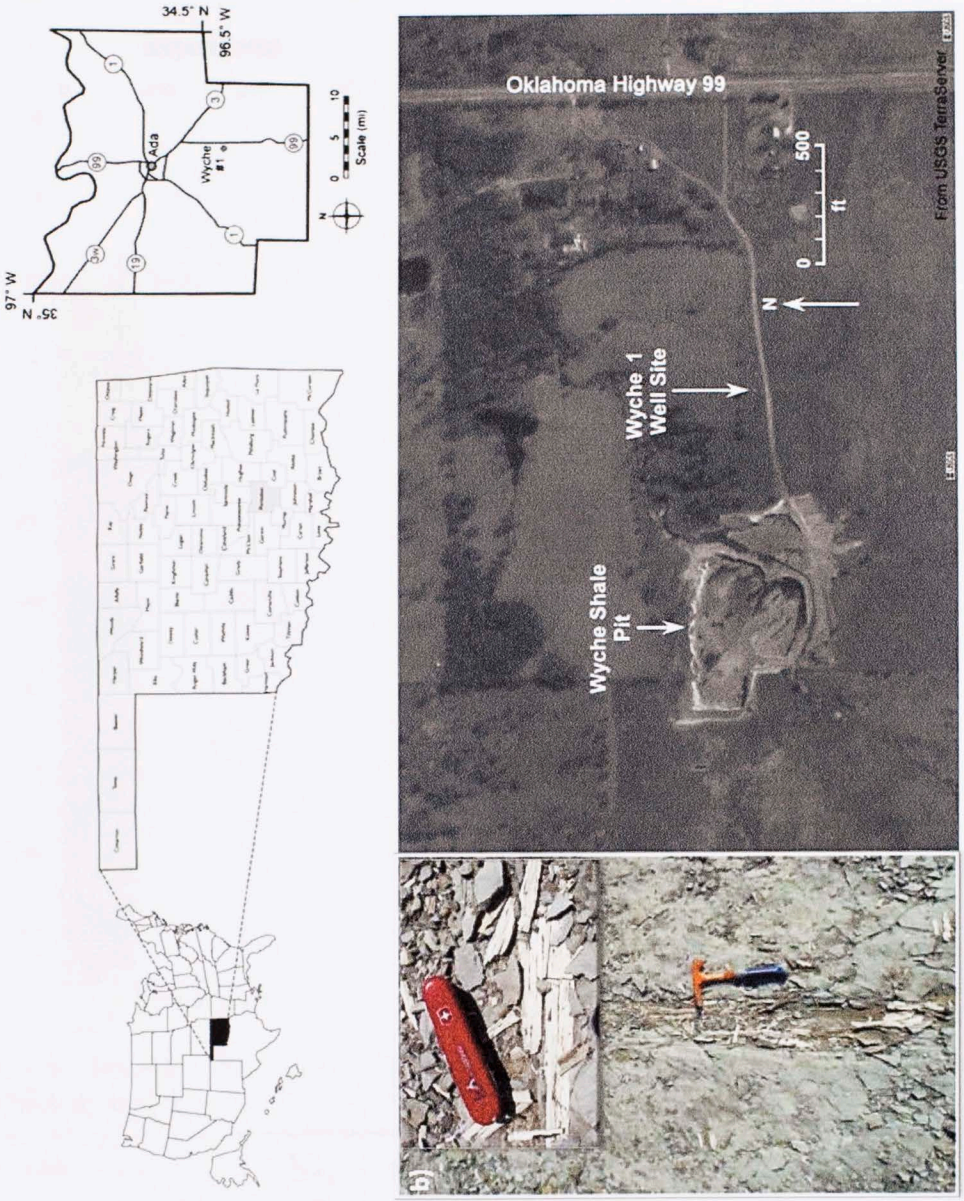

Figure 5. Map and images showing the location of the Wyche shale pit and well. Buckner et al., (2009); Miceli-Romero and Philp (2012). 5b) Silicified log found parallel to the bedding in the Wyche shale pit outcrop. This silicified and carbonized log was determined to be *Archaeopteris* (*Callixyon sp*), a Late Devonian tree (William Stein, pers. comm., 2012).

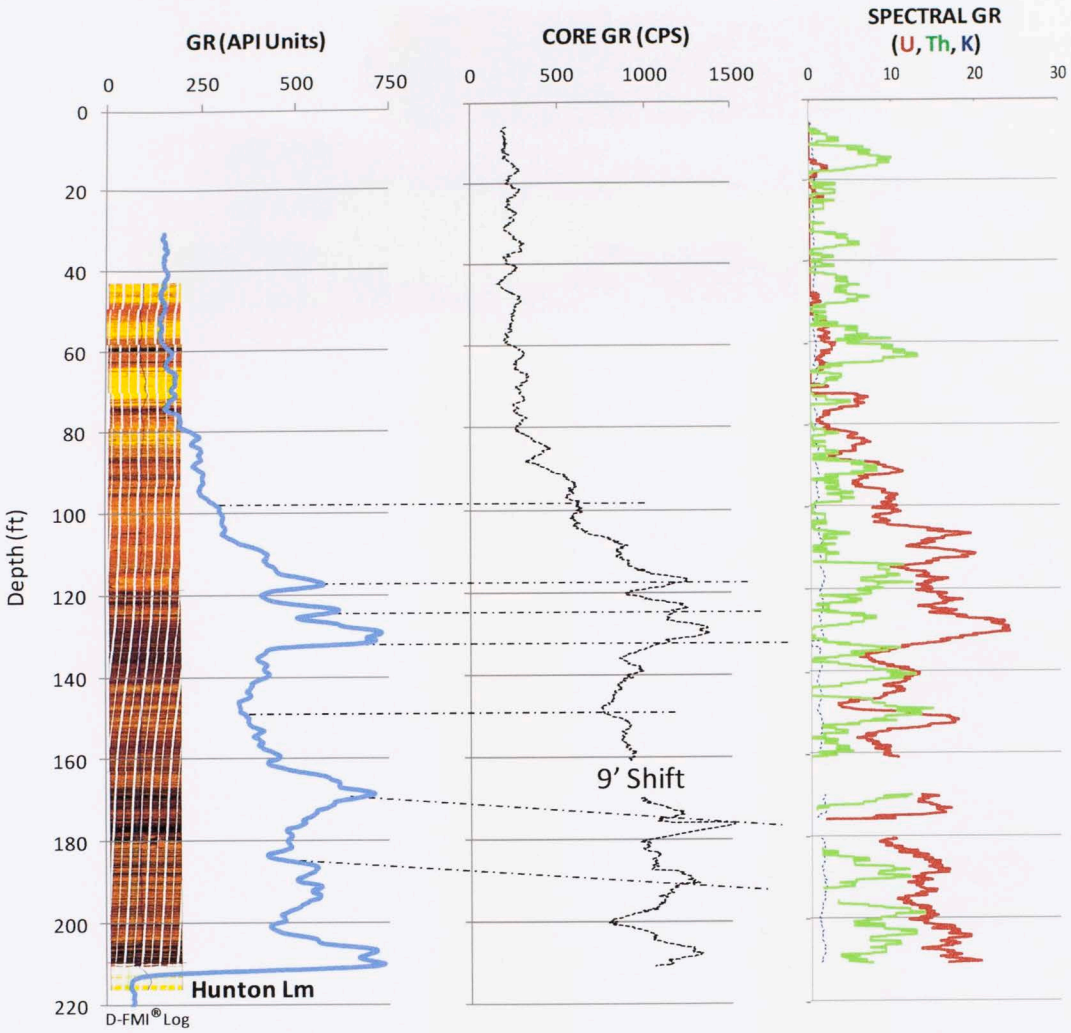

Figure 6. Gamma Ray (GR) well log, Dynamic Formation Micro Imager (D-FMI®) logs and Spectral Core Gamma Ray.

These logs were used for correlating the facies described in core with the Wyche-1 well logs (Notice the 9' shift beneath 160' depth). The GR signal seems mainly dominated by Uranium (U), instead of Thorium (Th) and Potassium (K) content.

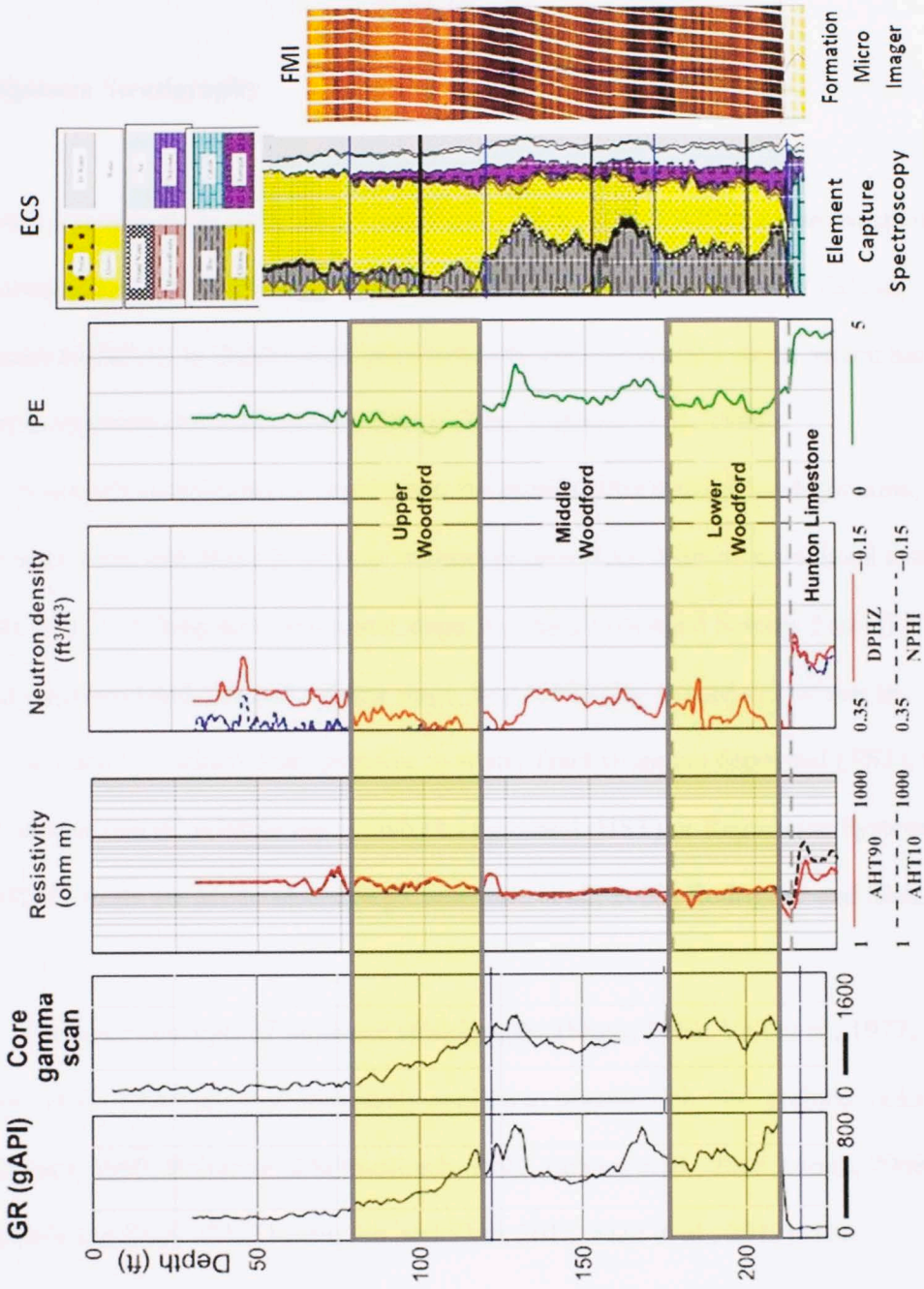

Figure 7. Borehole log data set from the Wyche-1 well.
After Abousleiman et al.(2007); Buckner et al.(2009); Portas (2009); Sierra et al. (2010); Slatt et al. (2012); Miceli-Romero and Philp (2012).

4. Methods

4.1 Sequence Stratigraphy

Sequence stratigraphy is the study of genetically related facies within a framework of chronostratigraphically significant surfaces. This technique is crucial in explaining lithofacies variations in depositional environments and recognizing strata, which are stacked in repeated and predictable patterns (Van Wagoner et al., 1990).

Sequence stratigraphy is based upon the premise that through geologic time, the oceans have risen and fallen in a cyclic manner (Figure 8A). A relative sea level cycle consists of: (1) a falling and turnaround stage, in which Lowstand Sytems Tract (LST) strata are accumulated, (2) and a rising stage, first exhibiting a rapid rate of rise in relative sea level, in which Transgressive Systems Tract strata are deposited (TST), and a later, slower rate of relative rise, in which Highstand (HST) or Regressive Systems Tract (RST) strata are accumulated (e.g.Catuneanu et al., 2009; Rodriguez and Slatt, 2012).

The basic concepts of sequence stratrigraphy (Sloss, 1963; Vail et al., 1977; Van Wagoner et al., 1990) are now commonly applied to organic rich, fine grained rocks (e.g. Bohacs, 1990; Bohacs and Schwalbach, 1992; Bohacs et al., 2005; Singh, 2008; Abouelresh and Slatt, 2012; Rodriguez and Slatt, 2012; Slatt et al., 2012). The characterization of organic-rich, fine-grained rocks is not as straightforward as working with coarser shelf deposits and depends on the physiographic setting where the organic-matter-rich rocks were accumulated: constructional shelf margin, platform/ramp or continental slope/basin (Passey et al., 2010).

In distal settings, the effects of changes in the base (sea) level are more subtle than in more proximal settings, but the interactions of eustasy, tectonic, accommodation space, sedimentary supply and climate may produce sequence stratigraphy patterns recognized even in relatively deep water deposits (Figure 8B).

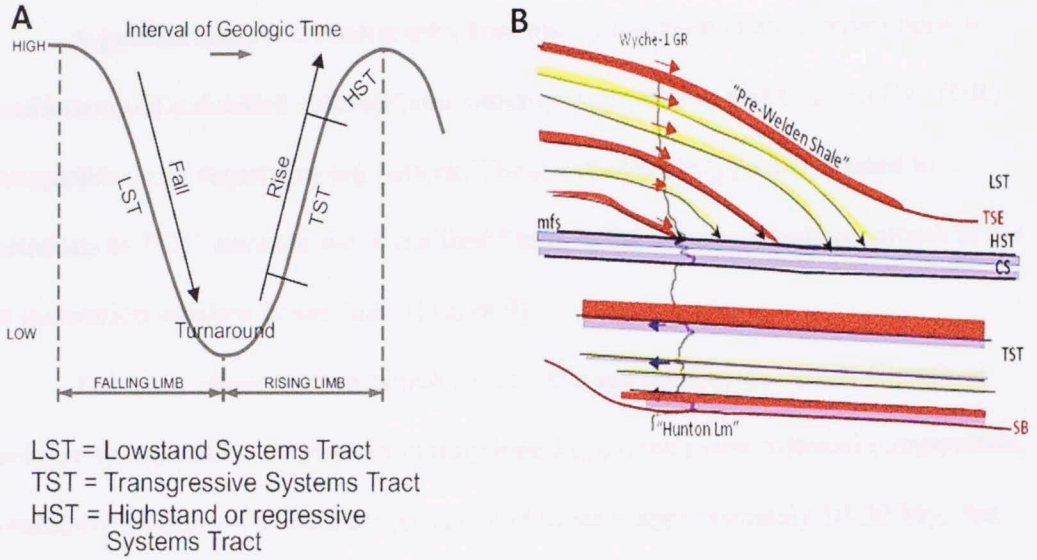

Figure 8. Sea level cycle and General Sequence Stratigraphic model for Late Devonian black shales.
Organic-rich shales rest on an unconformity surface, which is interpreted as a combined sequence boundary (SB), formed during a drop in sea level, followed by further erosion during early transgression to provide a transgressive surface of erosion (TSE). Then, organic-rich shales are accumulated directly at the TSE and exhibit a fining-upward trend ending at the shale with the highest organic content. This characteristic defines the maximum flooding surface (*mfs*), related to the most landward extent of the shoreline during the sequence evolution. Then, downlap surfaces are often characterized by sediments with higher accumulation rates, and lithofacies changing from detrital quartz rich shales (reverse coarsening upward), to clay rich shales (low energy), with a higher proportion of microfossils more distally. Red and Yellow colors represent potential reservoirs associated with high frequency regressive cycles. Purple color represents the intervals of transgression, characterized by higher TOC and often higher GR values (After Rodriguez and Slatt, 2012; Slatt and Abousleiman, 2011).

The sequences related to organic-rich, fine-grained rocks are characterized by a low to moderate detrital influx (Bohacs et al., 2005). The lowstands might be related to small increments in traction bottom-energy current features (e.g.O'Brien and Slatt, 1990; Slatt and O'Brien, 2011), but these features were not commonly recognized at the Wyche-1 core-well.

A general sequence stratigraphy framework has been created based upon a combination of a detailed outcrop/core, outcrop examination and Gamma Ray (GR) transgressive and regressive log pattern. These patterns are typically related to variations in TOC, because the Woodford Shale in the Wyche-1 well are closer to the oil generation window lower limit (Figure 9).

The time framework in which a complete sea level cycle occurs (length of geologic time), can be interpreted mainly based upon their (micro)fossil components, commonly organic-rich shale cycles are: 2nd order = approximately 10-30 My; 3rd order = approximately 1-5 My and 4th order = approximately 100,000-300,000 years.

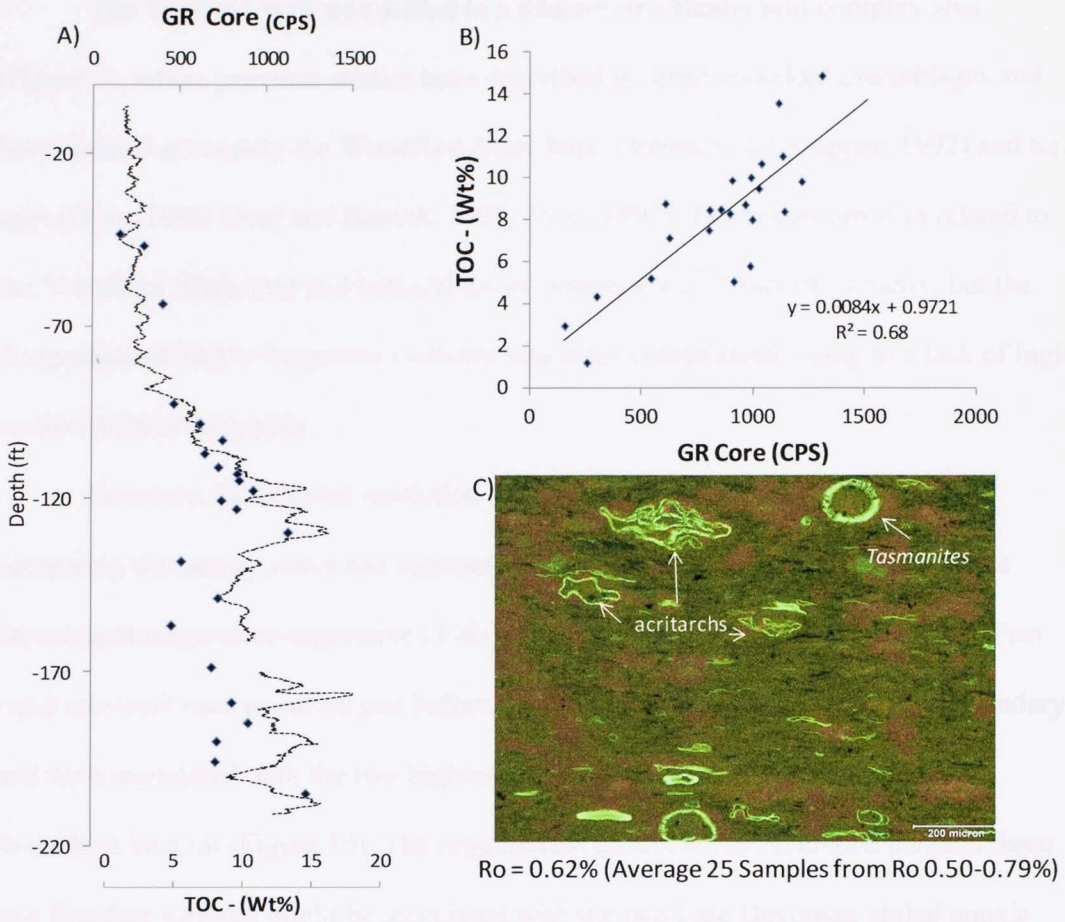

Figure 9. Core Gamma Ray (GR) and TOC content (Wt%) for the Wyche-1well. A). Core scan, in counts per second (CPS). B) The Positive correlation between the TOC content (Wt%) and GR core log may be related to the thermal maturity. Thermal maturity measurements taken from 25 samples from the Wyche-1 well illustrate that vitrinite reflectance percentage value ranges between 0.50 and 0.79 percent, with an average equal to 0.62 percent (Brian Cardott pers. comm., 2013). C) Thin section photo from the Wyche-1 well at 94.2 ft interval. The carbonaceous material fluoresces brightly (light green), under ultraviolet light and mostly includes possible acritarchs and *Tasmanites* that appear yellow under transmitted, plane polarized light. Patches of brown to yellow color represent intercrystalline microporosity, while the dark green areas denote non-porous areas (TOC Raw Data Courtesy Andrea Miceli-Romero; Thin Section Image courtesy TerraTeK and Devon Energy).

The Wyche-1 well was drilled in a relative structurally non-complex area (Figure 3), where previous studies have described in detail conodont assemblages and have defined accurately the Woodford Shale base (Johnson and Klapper, 1992) and top ages (Over, 1990; Over and Barrick, 1990; Over, 1992). The unconformities related to the Woodford Shale (top and bottom) limits comprise a 2nd order of cyclicity, but the designation of higher frequency cyclicity was more complicated owing to a lack of high resolution biostratigraphy.

However, the internal resolution for 3rd order cyclicity was established by comparing the transgressive and regressive pattern from Gamma Ray with the Late Devonian transgressive-regressive (T-R) cycles defined by Johnson et al.(1985). Two rapid sea-level rises occurred just before, and one at, the Frasnian-Famennian boundary and were associated with the two highest GR picks at the Wyche-1 core middle Woodford interval (Figure 10). The organic-rich sediments accumulated beneath these two flooding surfaces might be associated with the two Late Devonian global anoxic events known as the Upper and Lower Kellwasser events (McGhee, 1996; Walliser, 1996; Over, 2002). The Late Devonian T-R cycles seem to have been formed in response to mid-plate thermal uplift and submarine volcanism, while continental glaciation could have been a major factor in sea-level fluctuations during the Famennian Stage (Johnson et al., 1985).

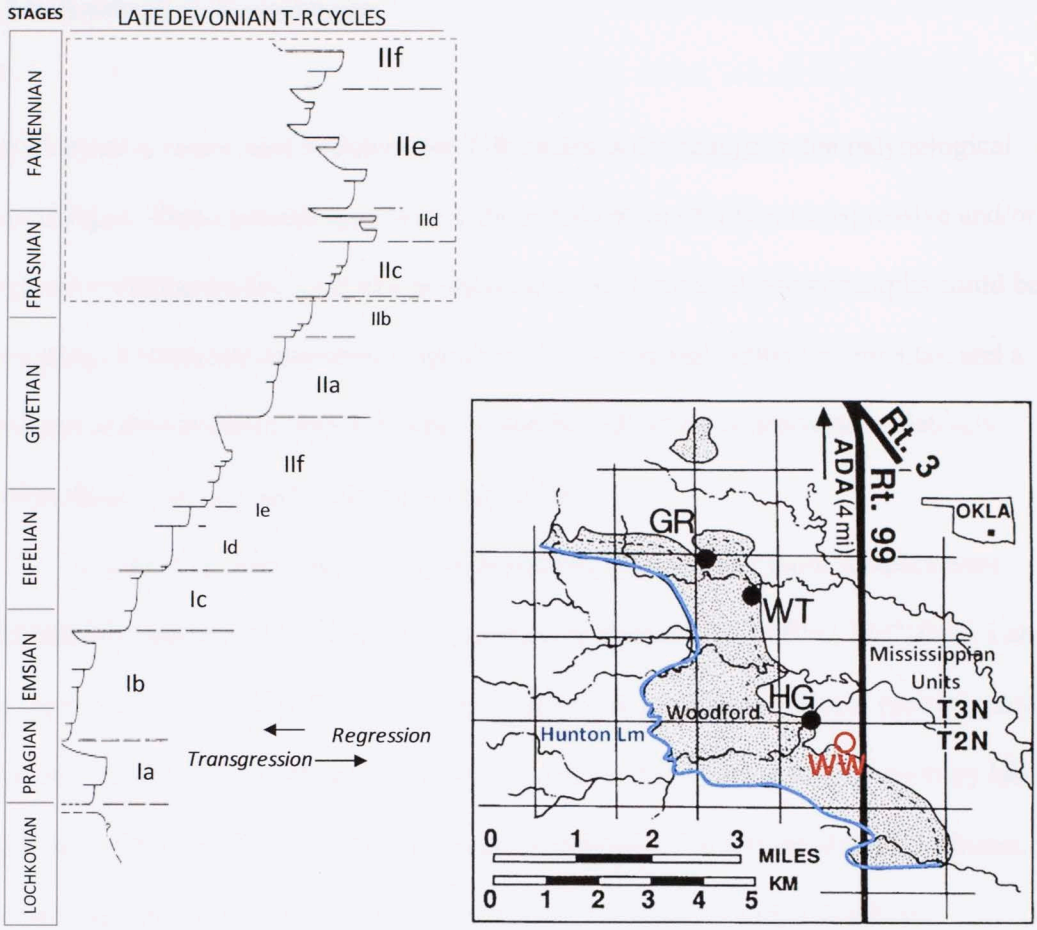

Figure 10. Transgressive and regressive cycles defined for the Devonian time. Devonian cycles recognized in the western United States, western Canada, New York, Belgium and Germany (Johnson et al., 1985). The highlighted rectangle represent the age interval associated with the Woodford Shale age reported from the Lawrence Uplift (Over, 1990; Over and Barrick, 1990; Over, 1992; Johnson and Klapper, 1992). The map illustrates the Woodford Shale outcrop belt on the Lawrence Uplift, and reference sections with detailed biostratigraphic conodonts studies: GR = Guest Ranch Section, WT = Welden Type Section, and HG = Hass G Section. WW = Wyche well and shale pit (After Ritter, 1990).

4.2 Palynological Assemblages

An alternative proxy used to determine T-R cycles is the change in the palynological assemblages. These assemblages were used as indicative of minor transgressive and/or regressive marine cycles, such that an increase in the terrestrial palynomorphs could be indicative of relatively near-shore deposition (or continental influx increments), and a decrease in the terrestrial palynomorphs could be indicative of deposition relatively farther from shore (or declining continental influx).

A total of 21 core intervals were previously selected and these samples were subjected to standard palynological preparation techniques by PALEO TECHNIC Lab Services. Eighteen (18) of these 21 samples provided good palynological recovery and were analyzed using a Carl Zeiss light microscope at the Petrographic microscopy lab in the ConocoPhillips School of Geology and Geophysics, The University of Oklahoma. At least one complete oxidized slide per sample was scanned with a 40x Zeiss planochromatic objective and 300 palynomorphs were counted per slide, when possible (Appendix 1).

The Pollen Index (PI) was calculated for 18 samples. The Pollen Index (PI) is here defined as the difference between one and the proportion of the pollen and spores grains in three hundred palynomorphs counted:

Pollen Index (PI): 1 - (Pollen and spores / Pollen and Spores + *Tasmanites* + acritarchs)

Palynomorphs were categorized in three groups: 1). Pollen and spores, 2). acritarch cysts and 3) *Tasmanites*. *Tasmanites* were differentiated from acritarchs by being thicker walled -cysts with radial pore canals (Figure 11).

A discussion about the algae nature of *Tasmanites* has been maintained by palynologists and micropaleontologists for many year (e.g.Tappan, 1980). However, now it is recognized that *Tasmanites* are associated with the cyst of *Prasinophycean* (primitive green) algae (Guy-Ohlson, 1988). The *Prasinophycean* algae presence in the water column is believed to be restricted by high water temperatures in the photic zone, and also *Prasinophycean* algae blooms have been related to enrichment of the water by nitrogen and phosphates (e.g.Vigran et al., 2008).

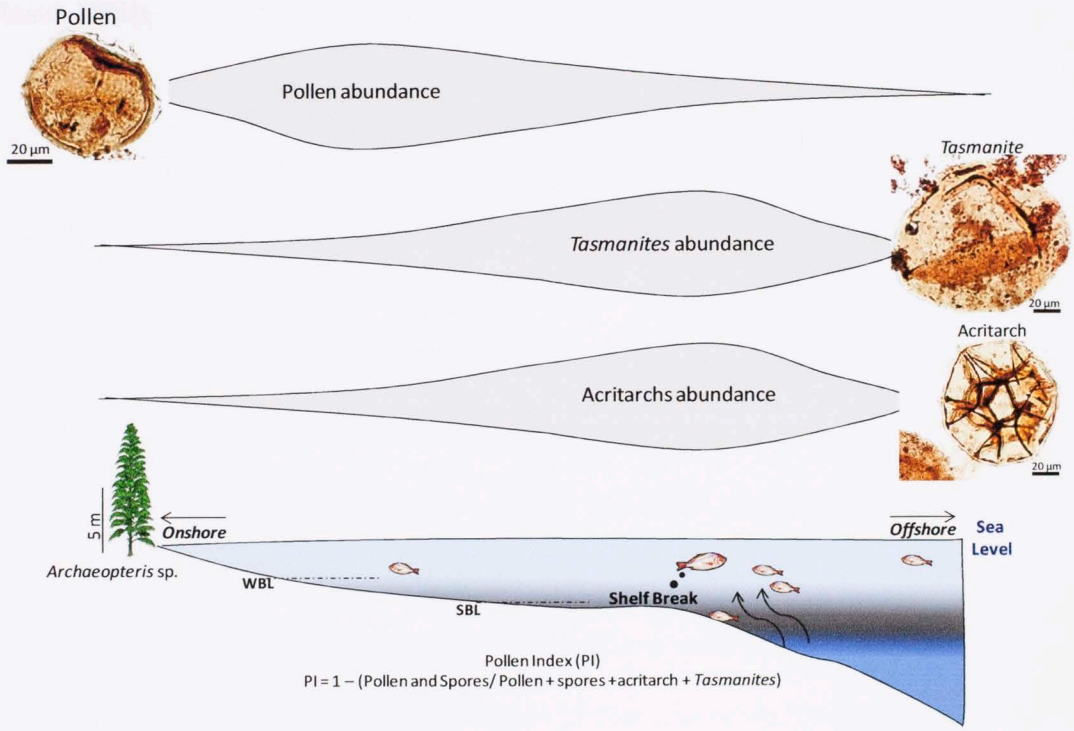

Figure 11. Changes in the Pollen Index (PI) as indicative of transgressive and/or regressive marine cycles.
Increments in the PI ratio could have been indicative of deposition nearer shore (or increasing continental influx) and a decrease could have been indicative of deposition farther from shore (or declining continental influx). The acritarchs were differentiated from *Tasmanites* because they are thicker walled -cysts with radial pore canals. WBL represents the wave base level and SBL is the storm base level.

Additionally, acritarchs life cycles seem to be related to the photic zone (Evitt 1963a; b). Due to their wide distribution and occurrence in a range of lithologies and facies, it is suggested that acritarchs were planktonic organisms (Molyneux et al., 1996). Planktonic organisms are not good paleo-depth indicators or shoreline distance markers (Strother, 1996). However, in combination with well known terrestrially-derived palynomorphs, they have been used for tracing transgressive/regressive cycles from Paleozoic deposits (e.g.Smith and Saunders, 1970; Jacobson, 1979; Richardson and Rasul, 1990).

4.3 Ti/Al and Si/Al ratios

Late Devonian organic-rich black shale could have experienced changes in continental sediment influx, producing variation in the Titanium/Aluminum (Ti/Al) and the Silica/Aluminum (Si/Al) ratios in the rock geochemical composition (e.g.Rimmer et al., 2004; Lash and Blood, 2011).

Particularly, the Ti/Al ratio has been used as an indicator of siliciclastic grains, because Al occurs in clay minerals, whereas Ti occurs both in clays and in sand- and silt-sized grains such as ilmenite, rutile, and augite (Schmitz, 1987). Thus, a higher Ti/Al may suggest the presence of Ti-containing coarser-grained minerals, which could be related to regressive cycles and negatively correlated with organic (or GR log) content (Figure 12).

The Si/Al ratio has also been used as a proxy for detrital influx (e.g.Rimmer et al., 2004). However, biogenic quartz may have been an important contributor to black shales and some reports consider that between 50 - 100% of the quartz silt in Late Devonian black shales is not detrital in origin and was precipitated early during diagenesis, possibly from biogenic quartz derived from radiolarians (Schieber, 1996).

This scenario makes the Si/Al ratio a questionable proxy for delimiting T-R cycles. However, lowstands can also be reflected by increasing biogenic quartz in response to increments in biological productivity (e.g.Bohacs et al., 2005). For that reason, Si/Al ratios were not discarded as a T-R marker and were analyzed together with TOC content, Ti/Al ratios, palynological assemblages and petrographic thin sections.

The Si/Al ratios tend to be positively correlated with the organic (or GR log) content when quartz increments of biogenic origin; but Si/Al ratios may be negatively correlated with the organic content when organic matter is diluted by continental detrital input (Figure 12).

The Ti, Al, and Si contents were analyzed on the Element Capture Spectroscopy (ECS) log. The ECS log from the Wyche-1 well has been compared with X-ray diffraction (XRD) mineralogy analysis and the differences between the two methods were not noteworthy (Abousleiman et al., 2009; Sierra et al., 2010). Further, the contribution of siliceous cement derived from volcanic ash and recrystallization of clay minerals was considered insignificant volumetrically, on the basis of petrographic examination.

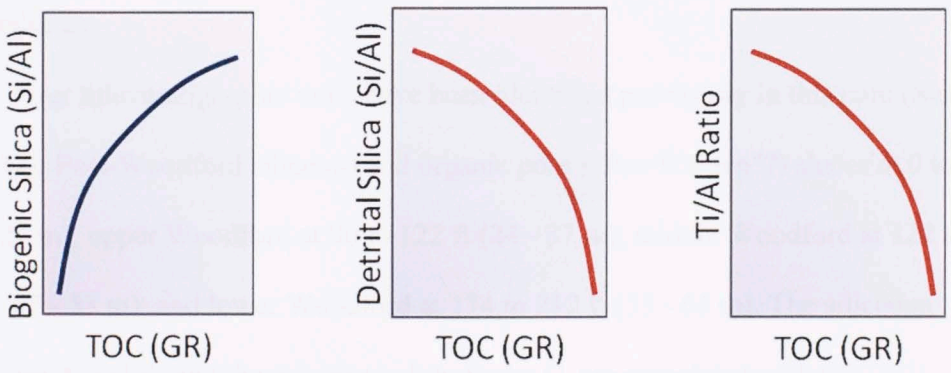

Figure 12. Possible variation of the Si/Al and Ti/Al ratio with respect to the Total Organic Carbon (TOC) or Gamma Ray (GR) log in immature rocks.
The Si/Al ratio tends to be positively correlated with TOC when silica is associated with biogenic quartz, while Si/Al ratio is negatively correlated with TOC when silica is related with a detrital origin. Ti/Al is normally negatively correlated with TOC because Al occurs in clay minerals, whereas Ti occurs both in clays and in Ti-containing minerals associated with coarser-grained sediments and increments in the continental detrital input (After Rimmer et al., 2004).

5. Results

5.1 Lithofacies Description

The Wyche-1 core description, core photographs, thin sections petrography, XRD mineralogy, geochemical analysis and wire-line log data, have led to the identification of nine lithofacies: (A) Siliceous laminated mudstone, (B) Light-gray, siliceous, finely laminated mudstone, (C) Light-gray, siliceous/argillaceous, calcareous mudstone, (D) Siliceous/argillaceous, finely laminated mudstone with phosphate and pyrite nodules, (E) Siliceous/argillaceous, laminated mudstone with phosphate nodules, (F1) Black to dark gray, laminated argillaceous mudstone, (F2) Black to dark gray, finely laminated argillaceous mudstone, (G) Mixed siliceous/argillaceous mudstone with thin clay laminations, and (H) Argillaceous siltstone with abundant angular detrital quartz (Appendix 2).

Four lithostratigraphic units have been identified previously in this core (Slatt et al., 2012): Post-Woodford siliceous and organic poor ("Pre-Welden"?) shales at 0 to 80 ft (0 - 24 m); upper Woodford at 80 to 122 ft (24 - 37 m); middle Woodford at 122 to 174 ft (37 - 53 m); and lower Woodford at 174 to 212 ft (53 - 65 m). The siliceous lithofacies A and B, and the calcareous lithofacies C are associated with the Mississippian "Pre-Welden Shale". The lithofacies D and E are generally identified with the upper Woodford interval. The organically richest lithofacies F1 and F2 are associated with the middle Woodford, while the quartz rich lithofacies G and H are commonly related to the lower Woodford (Figure 13).

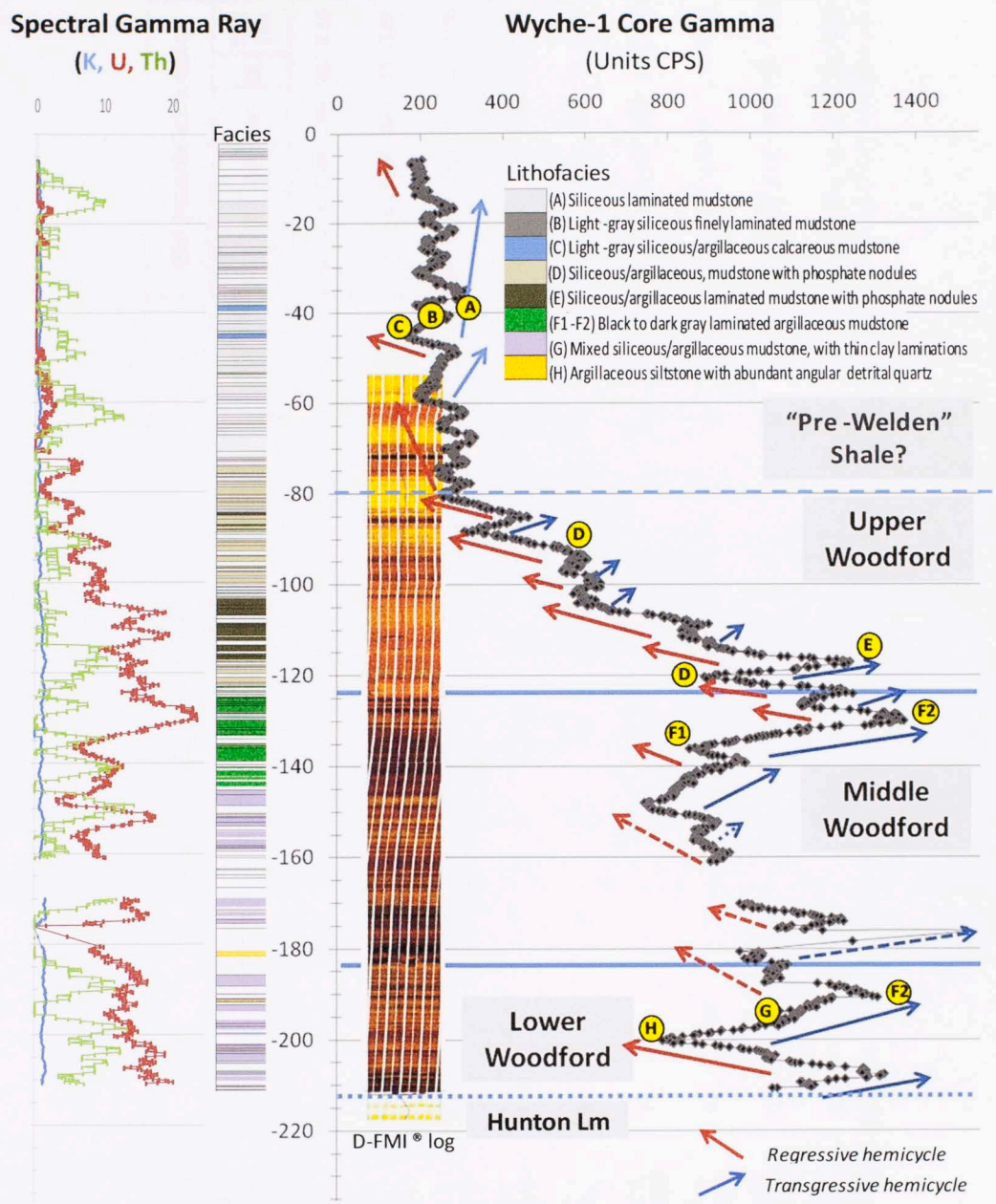

Figure 13.Lithofacies identified in the Wyche-1 core.

Notice that the Core Gamma Signal (CPS Units) is correlated with the Uranium (U) profile more than with the Potassium (K) and Thorium (Th) profiles. Red arrows represent regressive cycles and blue arrows represent transgressive cycles. Dashed lines represent unconformities at Woodford Shale Top and Bottom.

Table 1. XRD analysis for the lithofacies defined from the Wyche-1 well. Depth = Depth in core of each sample analyzed. Geochemical raw data, courtesy Andrea Miceli-Romero and Paul Philp.

Lithofacies	Depth (ft)	XRD – Mineralogical Composition										TOC (%) AND ROCK EVAL					
	XRD (Rock-Eval)	Quartz (%)	K-Feldspar (%)	Plagioclase (%)	Dolomite (%)	Siderite (%)	Gypsum (%)	Hematite (%)	Pyrite (%)	Illite/ Mica (%)	Kaolinite (%)	S1	S2	S3	HI	OI	TOC (%)
A	62.2 (62.2)	64	0	4	0	1	0	0	0	27	4	0.46	4.10	0.94	346	81	1.16
B	44.2 (44.2)	74	0	4	0	0	0	0	1	18	4	0.25	10.68	0.45	367	15	4.67
C	41.1 (41.2)	65	1	3	2	0	0	0	1	25	4	0.57	24.55	0.66	571	15	1.96
D	94.2 (92.3)	77	0	3	0	0	0	0	1	20	0	1.05	33.34	0.55	646	11	2.1
E	117.2 (118)	66	1	2	0	0	0	0	1	27	3	2.75	66.67	0.53	608	5	8.3
F1	134.5 (139.1)	52	1	4	9	0	0	0	3	27	4	1.60	33.78	0.58	589	10	5.74
F2	129.5 (123.3)	65	0	1	0	0	0	0	3	31	0	2.06	56.28	0.58	576	6	9.77
G	156.3 (157.8)	60	0	4	9	0	0	0	2	21	4	1.32	29.00	0.55	579	11	5.01
H	174.3 (181.1)	54	2	5	4	0	0	0	1	28	6	2.68	47.68	1.18	506	13	9.42

In order to compare the variation for the lithofacies defined from the Wyche-1 well, the XRD mineralogy and geochemical analysis are compiled in Table 1. S1= free volatile hydrocarbons content (mg HC/g rock); S2= remaining potential (mg HC/g rock); S3= organic carbon dioxide released (mg HC/g rock), Hydrogen Index = HI = S2 × 100/TOC, Oxygen Index = OI= S3 × 100/TOC.

The spectral gamma-ray log of the Wyche-1 core exhibits a dominance of the Uranium (U) signal with respect to the Potassium (K) and Thorium (Th) signals (Figure 13). The K- and Th- rich muddy deposits may suggest inheritance of minerals with terrestrial affinity while U- bearing minerals and high organic matter contents might represent muddy substrate under conditions of anoxia and slower sedimentation (Abouelresh and Slatt, 2012). U- has a high mobility and may be easily leached and redeposited in the subsurface which can make its distribution irregular, but TOC and palynomorphs assemblages seem to validate the oxygen poor and low sedimentation rate conditions.

Lithofacies A: Siliceous laminated mudstone.

Lithofacies A is characterized in thin section by yellow to brown compressed organic particles (*Tasmanites*), few dark brown to opaque carbonaceous stringers (C) and angular detrital quartz (q). Matrix is composed of finely layered clays and high amounts of finely disseminated quartz cement. Most of the quartz occurs as authigenic microcrystals (Chert) mixed within the clay matrix. Some possible radiolarian are observed; authigenic quartz (Cht) and authigenic pyrite (Py) are sparse or filling the cavities of some *Tasmanites*. XRD analysis shows a predominant quartz content (64%), with illite/mica (27%), and small amounts of kaolinite (4%), plagioclase (4%) and siderite (1%) (Figure 14).

The hydrocarbon (HC) potential for this interval is moderate, according to the Rock-Eval analysis. The S1, free volatile hydrocarbons content (free oil content thermally flushed from a rock sample at 300°C), is equal to 0.46 mg HC/g rock. The S2, remaining potential (HCs that crack during standard Rock-Eval pyrolysis temperatures), is equal to 4.01 mg HC/g rock. The S3, organic carbon dioxide released from rock samples, is equal to 0.94 mg HC/g rock. The total organic carbon (TOC) is equal to 1.16 %. The Hydrogen Index (HI = S2 × 100/TOC) is equal to 346 and the Oxygen Index (OI = S3 × 100/TOC) is equal to 81 (Table 1).

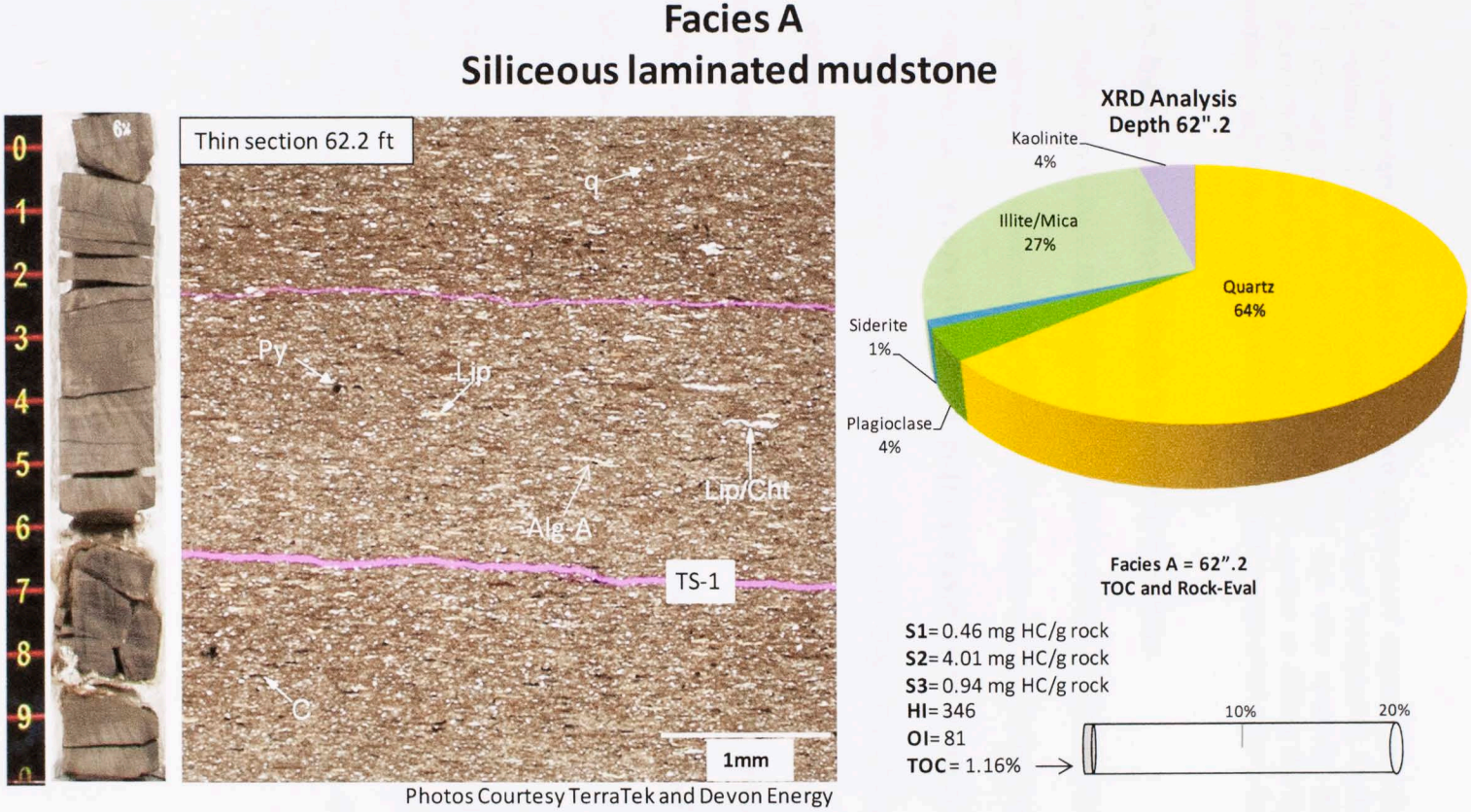

Figure 14. Lithofacies A, Siliceous laminated mudstone.

Lithofacies A is characterized by yellow to brown compressed organic particles related to Acritarch (Liptinite = Lip), and *Tasmanites* (Alginite A or Telalginite). Carbonaceous stringers (C) and angular detrital quartz grains (q) are also sparsely distributed. Authigenic quartz (Cht) and authigenic pyrite (Py) are sparse or filling the cavities of some *Tasmanites*. Purple lines are related to epoxy and may represent micro-fractures.

Lithofacies B: light-gray, siliceous, finely laminated mudstone.

Lithofacies B is characterized in thin section by reduced amounts of visible organic particles and carbonaceous stringers. The lithofacies B is also differentiated from lithofacies A by more laminations (Figure 15). Well laminated intervals exhibit highly siliceous (1-3 mm thick) laminae, characterized by authigenic quartz replacing *Tasmanites* and recrystallized radiolarians. Pyrite also fills some cavities.

The XRD analysis shows an increase in the quartz content (73%), and a reduction of illite/mica content (18%) with respect to lithofacies A. This lithofacies B also has a small amount of kaolinite (4%), plagioclase (4%) and pyrite (1%).The hydrocarbon generation potential for this interval is better than the lithofacies A. The free volatile hydrocarbons content (S1) = 0.25 (mg HC/g rock), the remaining potential (S2) = 10.68 (mg HC/g rock), the organic carbon dioxide (CO_2) released from rock samples (S3) = 0.45 (mg HC/g rock), the TOC = 4.67%, the Hydrogen Index (HI) = 367 and the Oxygen Index (OI) = 15 (Table 1).

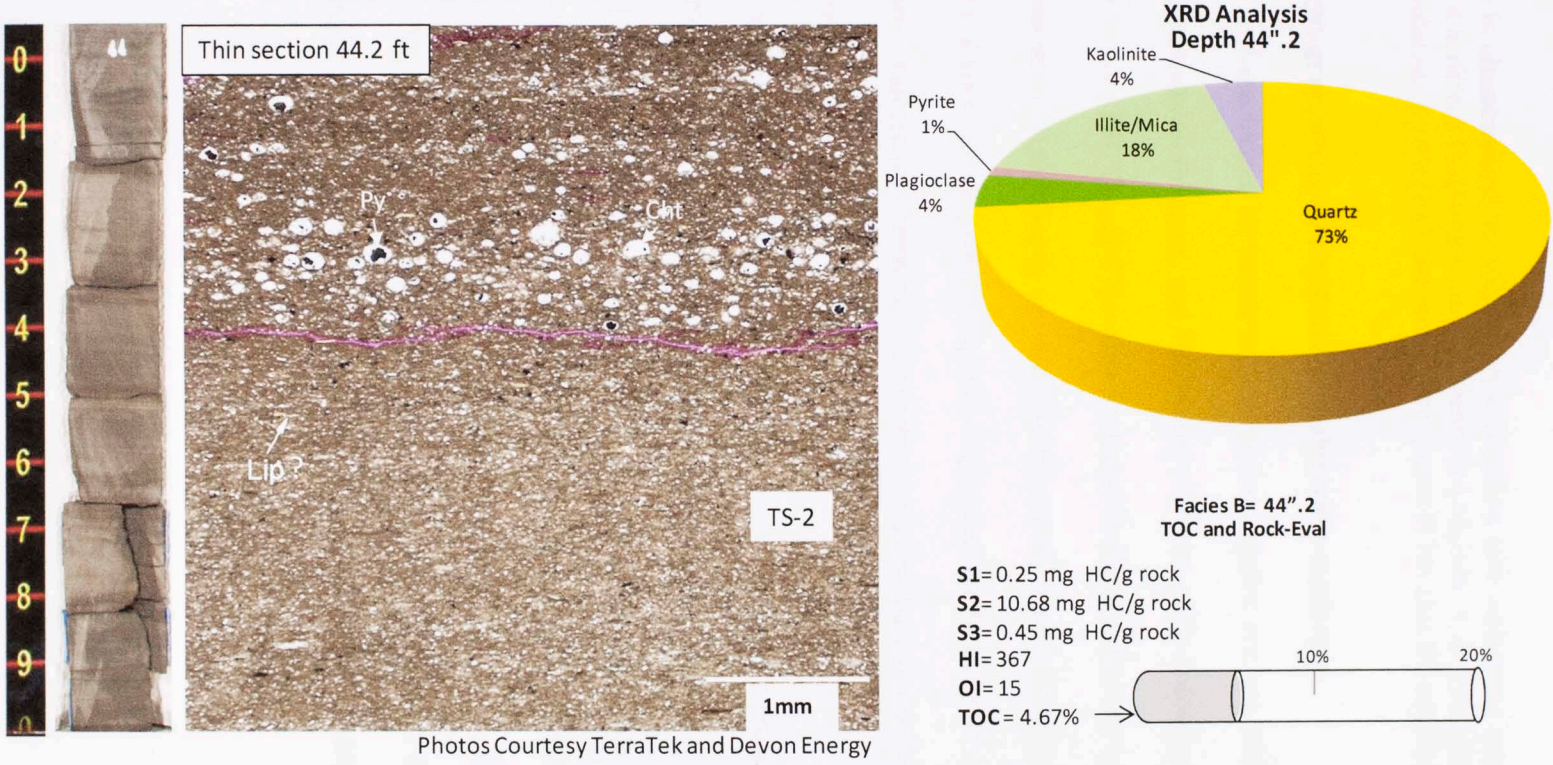

Photos Courtesy TerraTek and Devon Energy

Figure 15. Lithofacies B, light-gray siliceous, finely laminated mudstone.

The lithofacies B is characterized by increasing lamination and authigenic quartz that represents replaced acritarch (Liptinite=Lip), *Tasmanites* (Alginite A or Telalginite) and recrystallized radiolarian. Pyrite (Py) and authigenic quartz (Cht) also fill cavities.

Lithofacies C: light-gray, siliceous/argillaceous, calcareous mudstone.

This lithofacies C is characterized by increasing amounts of organic content, including *Tasmanites* and carbonaceous stringers, and also by the presence of Fe-dolomite (blue dolomite) crystals (Figure 16). The well laminated interval is characterized by wavy laminations (or burrows?). In most cases the microfossils are replaced with quartz, because the preserved structure suggests a biogenic origin, such as *Tasmanites* or radiolarians. Biogenic calcareous fragments are common and also partially replaced with pyrite and quartz.

The XRD analysis also shows the presence of dolomite (2%) and a predominant quartz content (64%), illite/mica (25%) and small amounts of kaolinite (4%), plagioglase (3%), k-feldespar (1%) and pyrite (1%) (Figure 16). The hydrocarbon potential for the lithofacies C is good to moderated: The free volatile hydrocarbons content (S1) = 0.57 (mg HC/g rock), the remaining potential (S2) = 24.55 (mg HC/g rock), the organic CO_2 release from rock samples (S3) = 0.66 (mg HC/g rock), the TOC = 1.96%, the Hydrogen Index (HI) = 571 and the Oxygen Index (OI) = 15 (Table 1).

Figure 16. Lithofacies C, Light-gray, siliceous/argillaceous, calcareous mudstone.

The lithofacies C is characterized by increasing amounts of organic content, possibly related to acritarchs (Liptinites=li) or *Tasmanites* (Alginite A or Telalginite), and carbonaceous stringers (C). Dolomite crystals (Fd) are common. Calcareous fragments are common and partially replaced with pyrite (Py) and authigenic quartz (Ct).

Lithofacies D: siliceous/argillaceous, finely laminated mudstone, with phosphate and pyritic nodules.

This lithofacies D is characterized by phosphate nodules that produce differential compaction and some fractures which are filled with quartz. The lithofacies D intervals are compact and characterized by reduced amounts of visible organic fragments and carbonaceous stringers. The organic particles are mainly filled with quartz and compacted in the highly siliceous intervals. These siliceous laminae are more prevalent than clay - carbonaceous laminae with a few scattered *Tasmanites*, commonly replaced partially with authigenic quartz (Figure 17).

The XRD data shows a predominant quartz content (76%), illite and mica (20%) and slight content of plagioclase (3%) and pyrite (1%). The HC potential for this lithofacies is good to excellent. The free volatile hydrocarbons content (S1) = 1.05 (mg HC/g rock), the remaining potential (S2) = 33.34 (mg HC/g rock), the S3 = 0.55 (mg HC/g rock), the TOC = 2.1%, the Hydrogen Index (HI) = 646 and the Oxygen Index (OI) = 11 (Table 1).

Figure 17. Lithofacies D, siliceous/argillaceous, finely laminated mudstone, with phosphate and pyritic nodules.

The lithofacies D is characterized by the organic particles filled with authigenic quartz (Cht) and phosphate nodules (*f*). The siliceous laminae are more prevalent than clay - carbonaceous laminae with a few scattered acritarchs (Lip) and *Tasmanites* (Alginite A or Telalginite).

Lithofacies E: siliceous/argillaceous laminated mudstone with phosphate nodules

This lithofacies E is characterized by visible organic material, darker appearance, sparse brown to orange phosphate bone particles and authigenic pyrite crystals. This lithofacies is also differentiated by decreasing finely disseminated detrital quartz, and authigenic quartz. Some well laminated intervals exhibit highly siliceous laminae (1-3 mm thick), characterized by cherty and pyrite concretions that represent replaced *Tasmanites* and recrystallized radiolarian. Pyrite lenses are also common and concentrated in narrow intervals (0.5-1 mm wide) (Figure 18).

The mineralogical composition based on XRD analysis is characterized by abundant quartz (66%), illite/mica (27%) and reduced amounts of kaolinite (3%), plagioclase (2%), K-feldspar (1%) and pyrite (1%). The HC potential associated with this lithofacies is excellent. The free volatile hydrocarbons content (S1) = 2.75 (mg HC/g rock), the remaining potential (S2) = 66.67 (mg HC/g rock), the organic carbon dioxide released from rock samples (S3) = 0.53 (mg HC/g rock), the TOC = 8.3%, the Hydrogen Index (HI) = 608 and the Oxygen Index (OI) = 5 (Table 1).

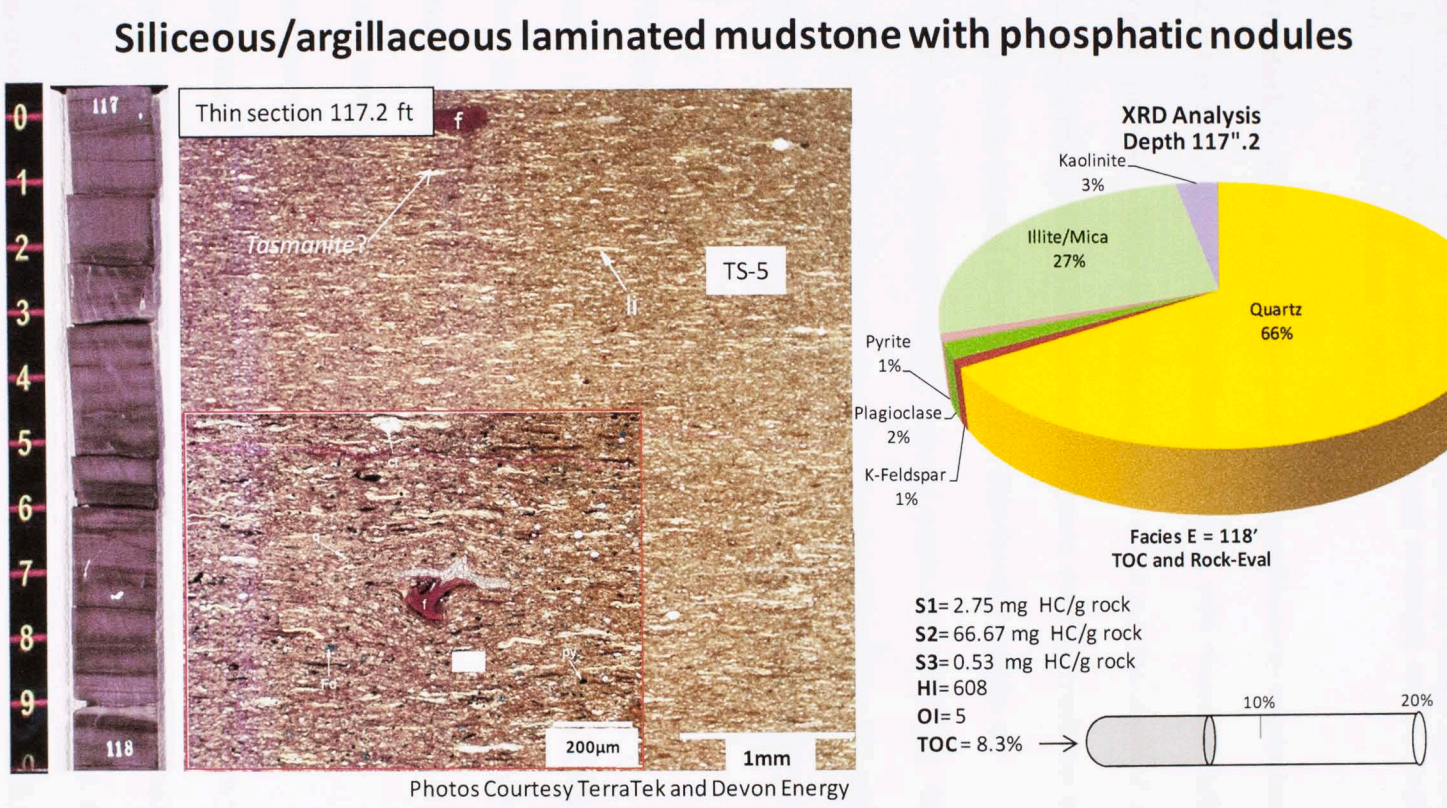

Figure 18. Lithofacies E, siliceous/argillaceous, laminated mudstone, with phosphate nodules.

The lithofacies E is characterized by visible organic material (li), darker appearance and sparse brown to orange phosphate particles (f). The red rectangle exhibits a phosphate particle partially replaced by authigenic quartz (Cht).

Lithofacies F1: black to dark gray, finely laminated, argillaceous mudstone

This lithofacies F1 is characterized by a argillaceous matrix, with abundant dark brown and opaque organic particles. These particles are sparse and some are rounded and filled with authigenic quartz and pyrite. Pyrite and detrital quartz occur in moderate amounts distributed throughout the interval (Figure 19). The lithofacies F1 rocks are characterized by abundant dolomite (9%) and reduced quartz content (52%). The plagioclase (4%) and kaolinite (4%) contents are higher than lithofacies F2, while the pyrite (3%) and k-feldspar (1%) amounts are similar between the lithofacies F2 and F1.

Lithofacies F2: black to dark gray, laminated, argillaceous mudstone

This lithofacies F2 is different from lithofacies E because of the absence of phosphate nodules and from the lithofacies F1 because of the reduced dolomite content and apparently fewer laminations. The laminated intervals are highly siliceous (1-3 mm thick), and characterized by authigenic quartz and pyrite which has replaced *Tasmanites* and recrystallized radiolarian (Figure 20).

The XRD data show a high quartz content (66%), illite/mica (31%), pyrite (3%) and reduced amounts of plagioclase (1%). The free volatile hydrocarbons content (S1) = 2.06 (mg HC/g rock), the remaining potential (S2) = 56.28 (mg HC/g rock), the organic carbon dioxide released from rock samples (S3) = 0.58 (mg HC/g rock), TOC = 9.77%, the Hydrogen Index (HI) = 576 and the Oxygen Index (OI) = 6 (Table 1).

Figure 19. Lithofacies F1, black to dark gray, finely laminated mudstone. The lithofacies F1 is characterized by a higher dolomite content, rounded Radiolarian and *Tasmanites* filled with authigenic quartz (Cht) and pyrite (Py). The detrital quartz (q) is less abundant and scattered. The magnification (red rectangle) exhibits the abundant Fe-dolomite content (Fd).

.

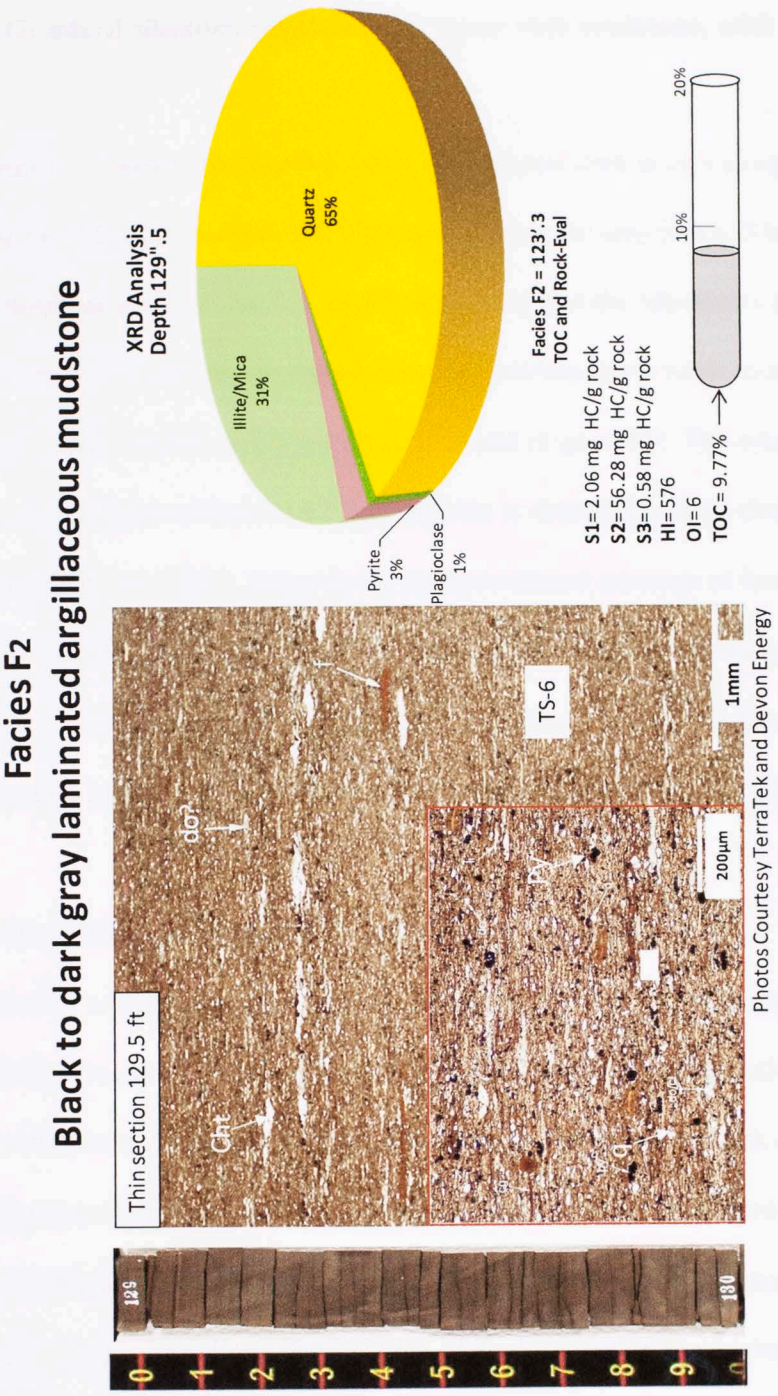

Figure 20. Lithofacies F2, black to dark gray, laminated argillaceous mudstone. The lithofacies F2 is characterized by the absence of phosphate nodules, apparently fewer laminations and the presence of abundant disseminated pyrite. The magnification (red rectangle) shows the absence of dolomite and abundant disseminated pyrite (Py).

Lithofacies G: mixed siliceous/argillaceous organic rich mudstone, with thin clay laminae.

This lithofacies G contains thin clay laminae and prevalent dark brown to opaque organic stringers. The lithofacies G is differentiated from the lithofacies D by the absence of phosphate nodules. Also, it is distinguished from the lithofacies F1 and F2, because of its more siliceous and compacted nature and because it hosts moderate amounts of dolomite, detrital quartz and quartz cement (Figure 21). The mineralogical composition of lithofacies G based on XRD analysis is characterized by abundant quartz (60%), illite/mica (21%), dolomite (9%), and reduced amounts of kaolinite (4%), plagioclase (4%) and pyrite (2%). The (S1) = 1.32 (mg HC/g rock), the remaining potential (S2) = 29.00 (mg HC/g rock), the (S3) = 0.55 (mg HC/g rock), the TOC = 5.01%, the Hydrogen Index (HI) = 579 and the Oxygen Index (OI) = 11 (Table 1).

Lithofacies H: greenish predominately argillaceous siltstone.

This lithofacies H contains abundant detrital angular quartz and dolomite crystals. There are a few Tasmanites, some which are replaced by quartz. Brown phosphatic fragments, sparse muscovite and authigenic pyrite are also present. Dark gray to black colored laminae are interlaminated with greenish siltstones, which are characterized by a high organic content (Figure 22). The XRD analysis shows the abundance of quartz (54%) and illite/mica (28%) contents and the presence of kaolinite (6%), plagioclase (5%), dolomite (4%), k-feldspar (2%) and pyrite (1%) (Table 1).

Figure 21. Lithofacies G, mixed siliceous/argillaceous, organic rich mudstone. The lithofacies G is principally differentiated from lithofacies D by the absence of phosphate nodules. It is also distinguished from lithofacies F1 and F2 because it is more siliceous and compacted, with a high content of dolomite.

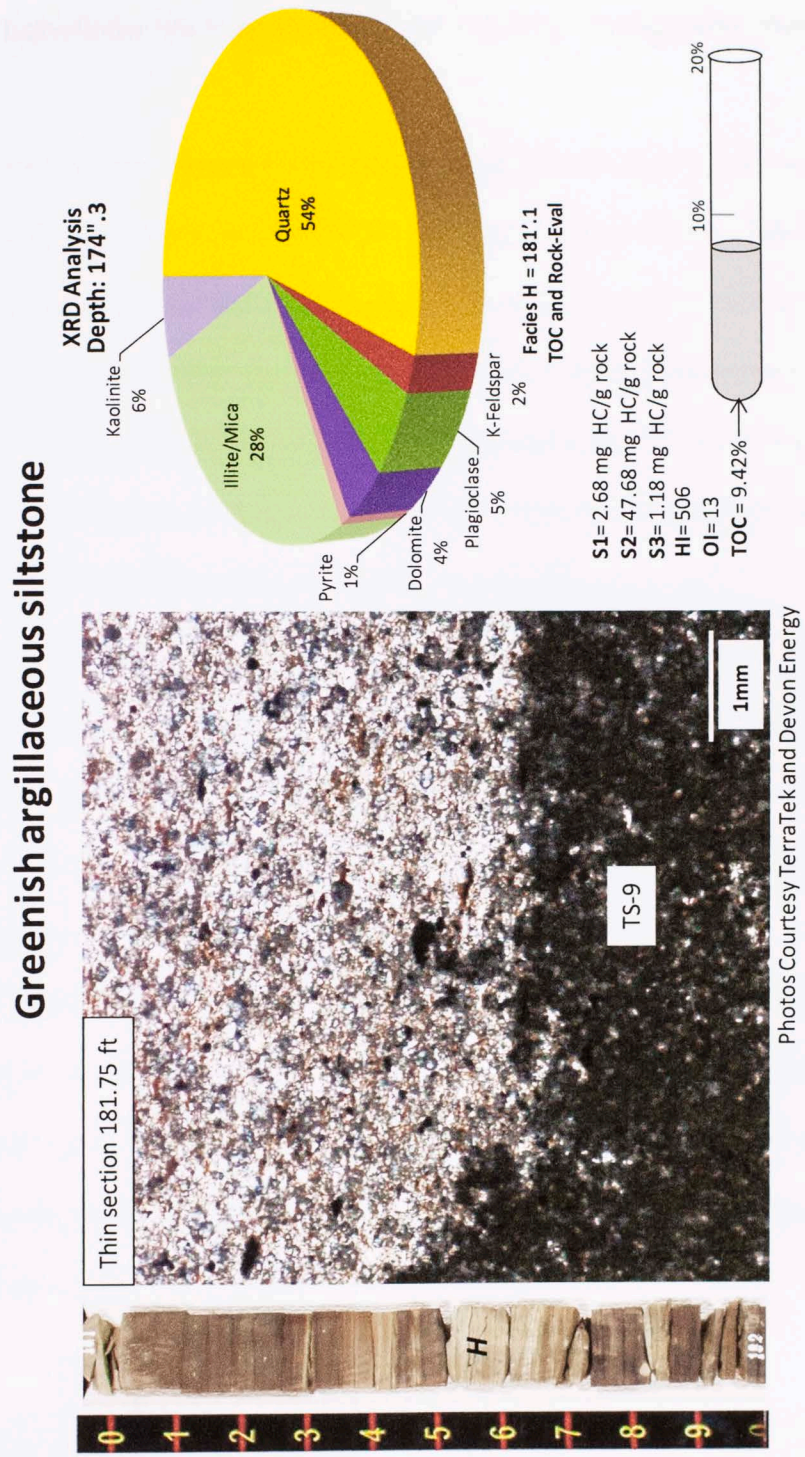

Figure 22. Lithofacies H, greenish predominately argillaceous siltstone. The lithofacies H is characterized by abundant detrital angular quartz and dolomite crystals , interbedding with dark gray to black colored laminae, characterized by a high organic content and a good hydrocarbon potential.

5.2 Wyche-1 Lithofacies Stacking Patterns and Sequence Stratigraphy Model

Some lithofacies stacking patterns in the Woodford and "Pre Welden" Shales were recognized during the detailed core lithofacies description. These repeated lithofacies stacking patterns were coupled with GR log variations: (1) "upward-decreasing" and (2) "upward-increasing", interpreted as: (1) regression and (2) transgression hemicycles. These regressive and transgressive hemicycles were grouped into 3rd order cycles; bounded by marine-flooding surfaces, characterized by high GR values (kick) and turnaround points of the lithostratigraphic stacking patterns.

The highest GR, organic-rich and phosphate-rich deposits comprise a 2nd order Condensed Section (CS), limited at the top by the 2nd order maximum flooding surface (*mfs*), that was used as a guide for labeling the 3rd order cycles (Figure 23).

In the Wyche-1well, the lower and middle Woodford is comprised of five 3rd order cycles which together exhibit a 2nd order transgressive (TST) pattern, characterized by upward-increasing GR log values, which are due to increasing organic-rich facies and the progressive occurrence of more distal (seaward) marine lithofacies (Figure 23). The upper Woodford contains six 3rd order cycles, which together present a 2nd order regressive (HST) pattern, differentiated by upward-decreasing GR log value and relatively more proximal (landward) lithofacies (Figure 23).

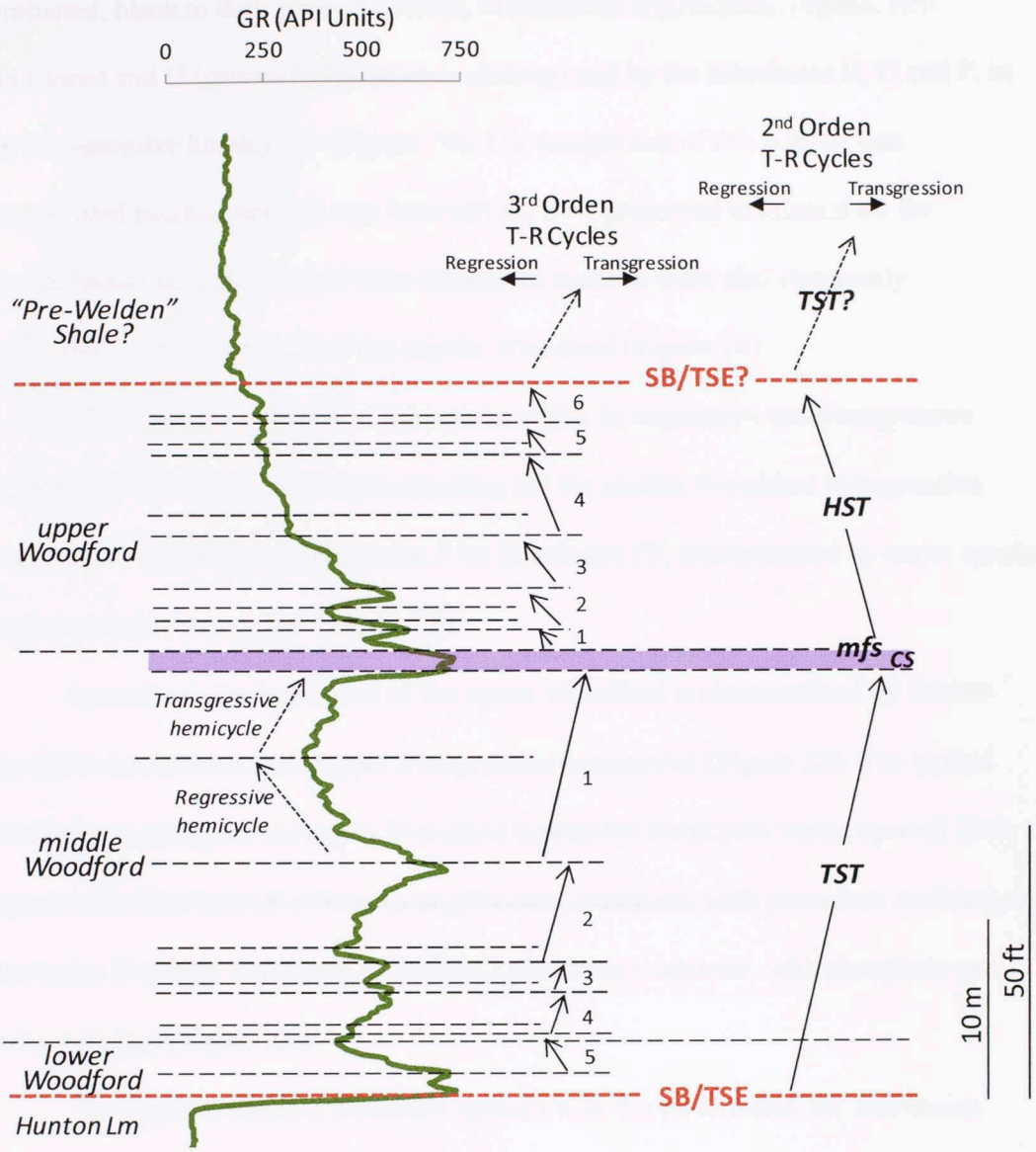

Figure 23. 2nd and 3rd Order cycles defined in the Wyche-1 well.
TST = Transgressive System tract, C3=Condensed Section; mfs= maximum flooding surface and HST=Highstand System Tract.

The lower Woodford is characterized by regressive and transgressive Gamma Ray hemicycles (Figure 23). The cyclic stacking pattern of lithofacies in the regressive hemicycles is typically represented upward by the lithofacies F(laminated and finely

laminated, black to dark gray mudstone), G (siliceous argillaceous, organic rich mudstone) and H (greenish argillaceous silstone) and by the lithofacies H, G and F, in the transgressive hemicycles (Figure 24). The recognition of this pattern was complicated because several core intervals are now preserved in mineral oil for geomechanics tests. However, these lithofacies patterns were also commonly recognized in the lower part of the middle Woodford (Figure 24).

The middle Woodford is characterized also by regressive and transgressive hemicycles. The typical lithofacies stacking for the middle Woodford transgressive hemicycle is upward from lithofacies F1to lithofacies F2, characterized by major quartz and lower dolomite content (Figure 25).

In contrast, the lower part of the upper Woodford is characterized by thicker regressive hemicycles and thinner transgressive hemicycles (Figure 25). The typical lithofacies stacking for the upper Woodford regressive hemicycle varies upward from organic-rich lithofacies E (siliceous/argillaceous mudstone, with phosphate nodules), to lithofacies D (finely laminated, siliceous/argillaceous mudstone, with phosphate and pyrite nodules) (Figure 25).

The upper Woodford continues upward with the pattern and the lithofacies stacking previously described. Above the "Pre-Welden", the gamma ray cyclicity changes and exhibits a higher frequency (Figure 26). The lithofacies stacking patterns are characterized by the lithofacies succession C (light gray, siliceous/argillaceous, calcareous mudstone), B (light gray, siliceous, finely laminated mudstone) and A (siliceous laminated mudstone), which presents a decreasing dolomite content, instead of increasing clay content (Figure 26).

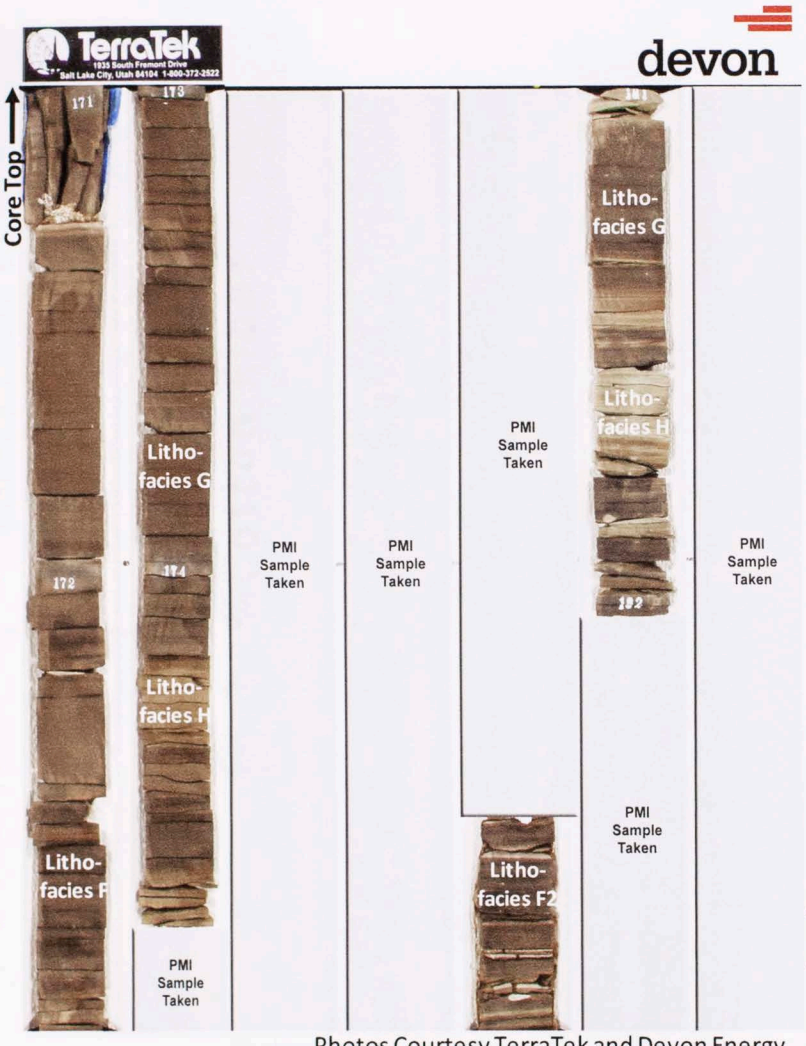

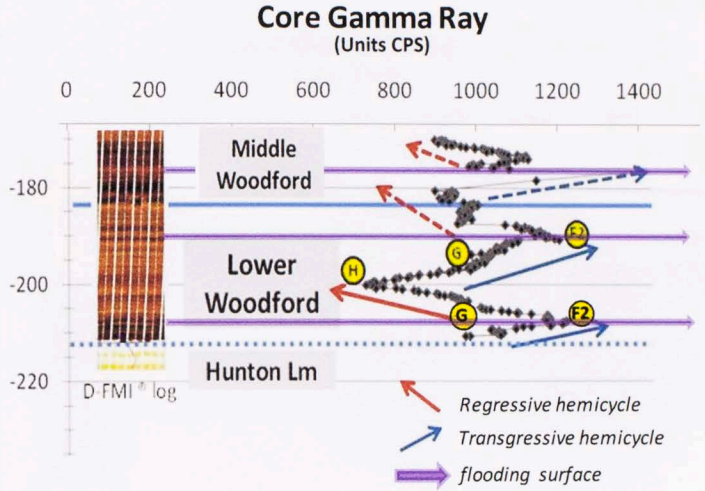

Lithofacies

(F1 -F2) Black to dark gray laminated argillaceous mudstone
(G) Mixed siliceous/argillaceous mudstone, with thin clay laminations
(H) Argillaceous siltstone with abundant angular detrital quartz

Figure 24. Gamma Ray and lithofacies stacking pattern identified in the lower Woodford.

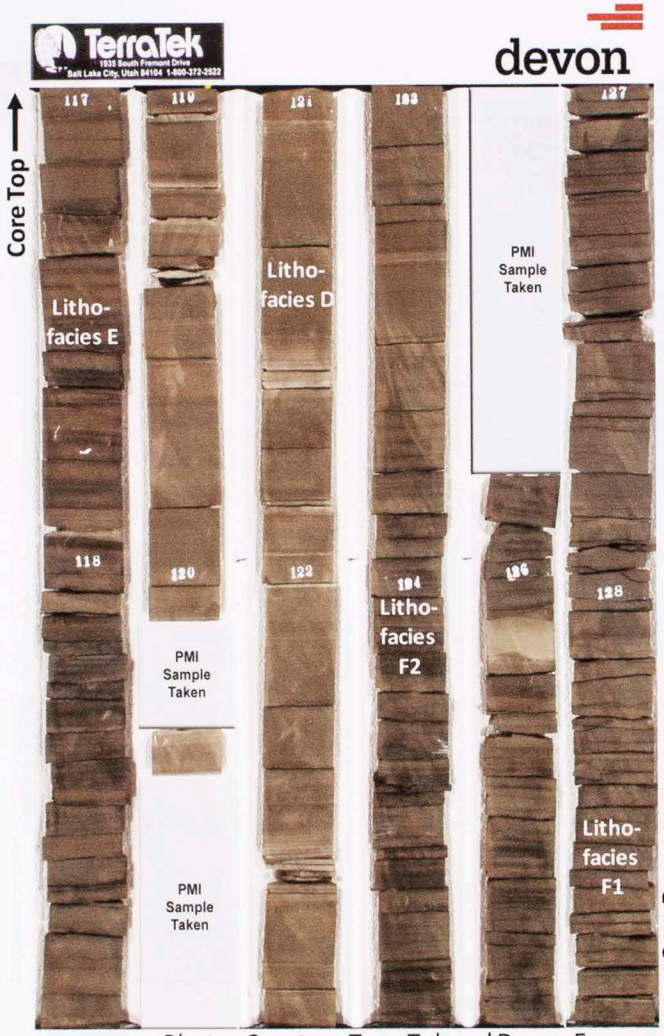

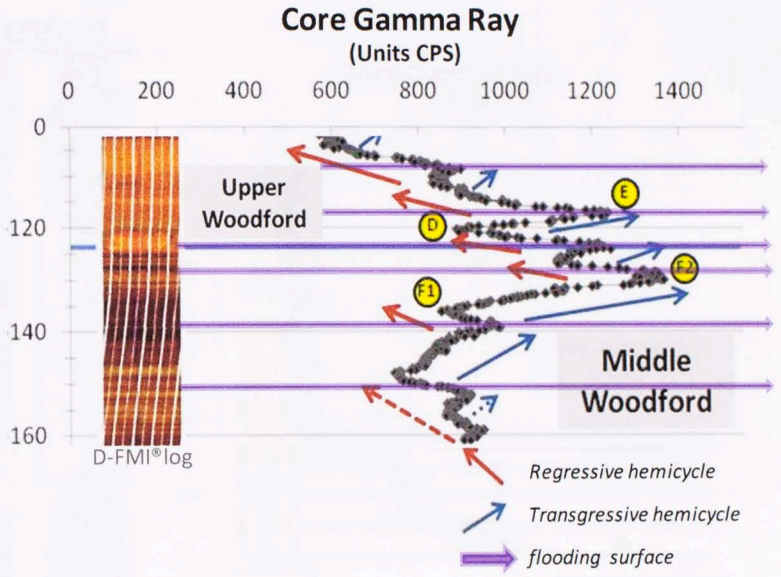

Lithofacies

(D) Siliceous/argillaceous, mudstone with phosphate nodules
(E) Siliceous/argillaceous laminated mudstone with phosphate nodules
(F1 -F2) Black to dark gray laminated argillaceous mudstone
(G) Mixed siliceous/argillaceous mudstone, with thin clay laminations

Figure 25. Gamma Ray and lithofacies stacking pattern in the middle Woodford and lower upper Woodford.

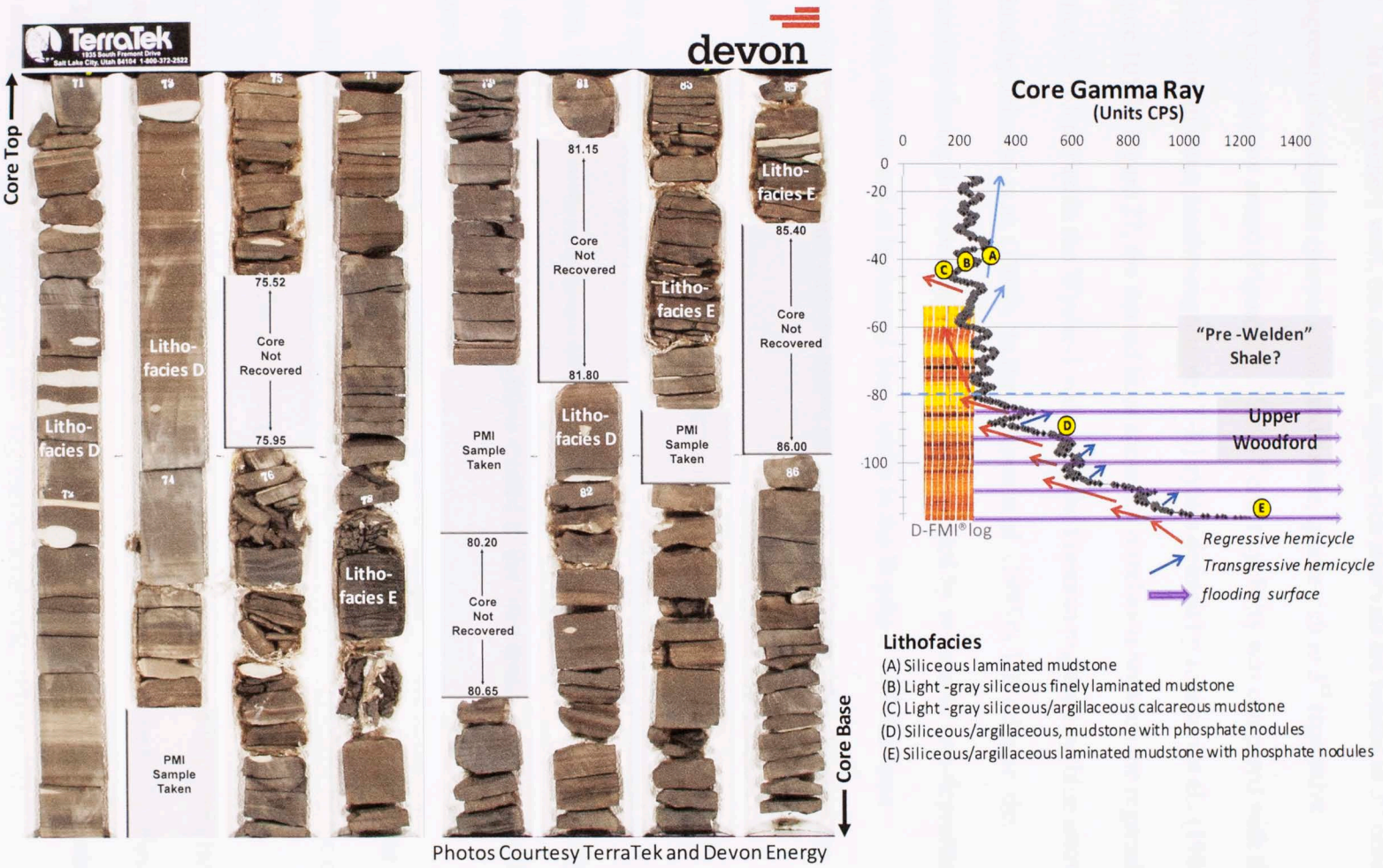

Figure 26. Gamma Ray and lithofacies stacking pattern in the upper Woodford.

In the Wyche-1 well, the ductile, organic-rich intervals are related to 3rd order transgressive hemicycles (purple areas) and brittle, quartz-rich to 3rd regressive hemicycles (yellow areas) (Figure 27). This 3rd order cyclicity was compared with the Late Devonian transgressive-regressive (T-R) cycles defined by Johnson et al., (1985) (Figure 10). In Figure 27, the dashed lines show the correlation between the regressive hemicycles identified in the Wyche-1 well, with the Frasnian regressions (blue arrows) defined by Johnson et al. (1985). In the Johnson et al. (1985)'s T-R scheme, the regressions during the Frasnian are possibly represented by erosion or non-deposition (diastem), represented as horizontal lines, while in the Wyche-1 well the same regression may correspond with the brittle intervals highlighted with yellow colors (Figure 27).

The dashed lines also show the correlation between the upper Woodford 3rd order regressive hemicycles, with the Famennian cycles defined by Johnson et al. (1985). The red arrows lengths are associated with the relative sea level fall intensity and the angle (or the vertical component) is related to the time span during sea level fall (Figure 27).

The 2nd order regressive HST is also subdivided into early (*E-HST*) and late (*L-HST*) Highstand Systems Tracts's (Figure 27). These intervals are separated by the onset of the base (sea) level fall (Onset-BLF) or the Correlative Conformity (CC *sensu*, Posamentier and Allen, 1999). The Onset - BLF represents the change in pattern from a normal regression (HST rising limb) to a forced regression (HST falling limb) (Figure 8). This event was characterized by changing the intensity of regression by increasing the red arrow angles of the 3rd order HST regressive hemicycles (Figure 27).

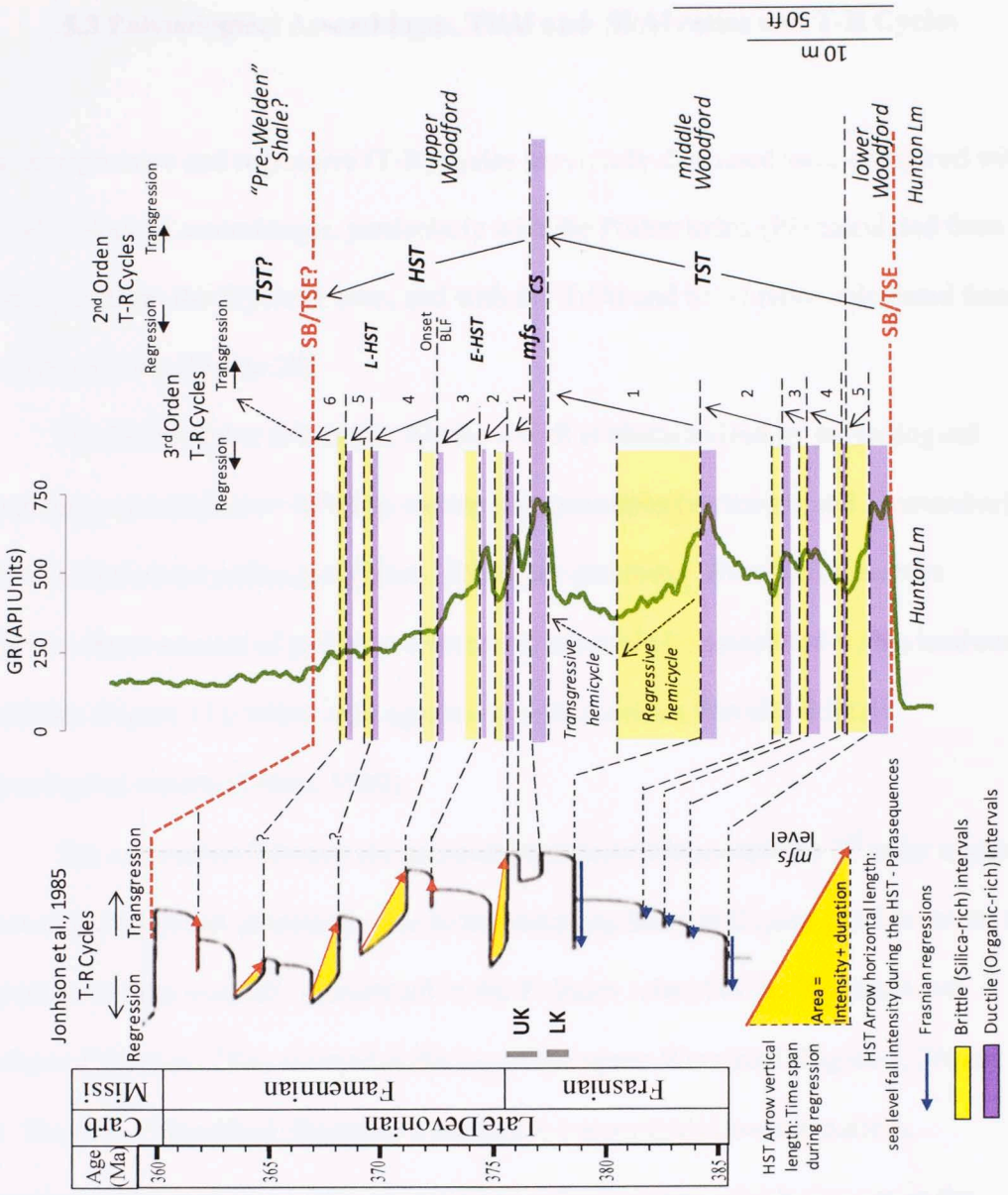

Figure 27. Sequence stratigraphy model for the Wyche-1 well.
SB = Sequence Boundary; TSE = Transgressive Surface of Erosion; TST = Transgressive System Tract; HST = Highstand System tract; *mfs* = maximum flooding surface; CS = Condensed Section; *E-HST* = Early - HST; *L-HST*= Late - HST; Onset BLF = onset of the sea (base) level fall; T-R cycles = Transgressive - Regressive cycles; UK = Upper Kellwasser event; LK = Lower Kellwasser event; age control after Over and Barrick (1990); Over (1992); and Johnson and Klapper (1992).

5.3 Palynological Assemblages, Ti/Al and Si/Al ratios and T-R Cycles

The transgressive and regressive (T-R) cycles previously discussed were compared with the palynological assemblages, particularly with the Pollen Index (PI) calculated from 18 samples from the Wyche-1 core, and with the Ti/Al and Si/Al ratios calculated from the ECS well log (Figure 28).

The Pollen Index (PI) in the Wyche-1 well is characterized by palynological assemblages dominated (> 80%) by marine palynomorphs (acritarchs and *Tasmanites*), instead of terrestrial pollen and spores. The upper and lower Woodford members present a major amount of pollen and spores which could be associated with a landward proximity (Figure 11); which is in agreement with previous Woodford Shale palynological reports (Urban, 1960).

The correlation between the palynological assemblages and the 3rd order cycles is not straightforward, principally due to the sampling interval (Figure 28). However, an important change is clearly recognized in the PI Index related to the Transgressive Surface of Erosion (TSE) situated at the top of the upper Woodford (Figure 4, 25 and 27). The upper Woodford illustrates a regressive (upward-shallowing) pattern, characterized by increasing-upward terrestrial palynomorphs, which changes in the "Pre-Welden" Shale to a transgressive (upward-deeping) pattern, characterized by a decreasing-upward terrestrial palynomorphs content (Figure 28).

In addition to the palynological assemblages, the Ti/Al ratios were also compared with the 3rd order T-R cycles. The Titanium contents are significantly higher with respect to Aluminum at the basal regressive 2nd order HST deposits, which

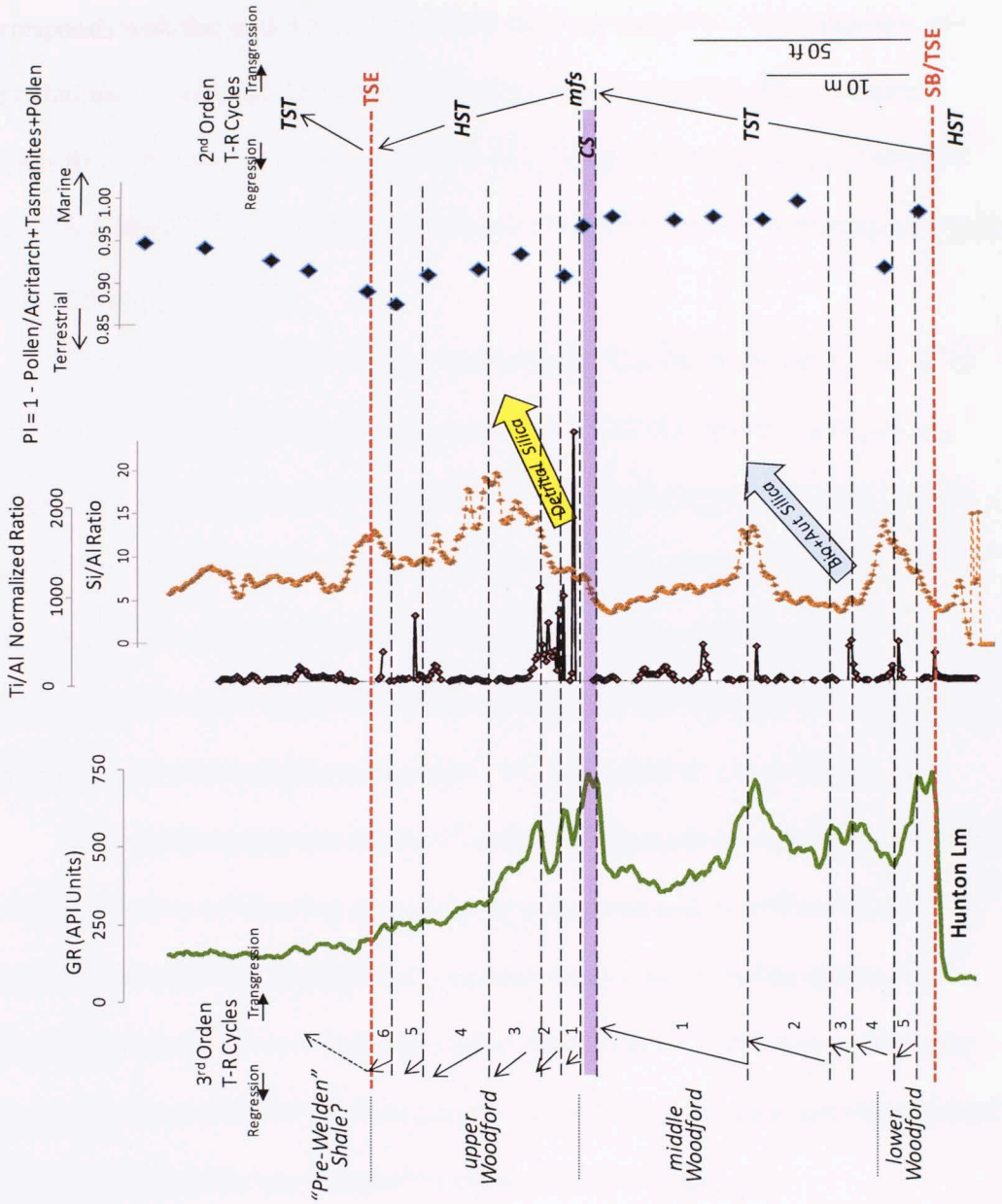

Figure 28. Transgressive-regressive (T-R) cycles, Pollen Index (PI), and the Ti/Al and Si/Al ratios calculated from the Wyche-1 ECS well log. The blue arrows represent a positive correlation between the Si/Al ratio and the Gamma Ray (GR) well log (API Units), while the yellow arrow shows a negative correlation between the Si/Al and the GR log.

corresponds with the shift between the (2nd order) transgressive (TST) deposits and aggradational Condensed Section (CS) deposits, to the regressive (HST) deposits (Figure 8). Ti/Al ratio peaks were also normally recognized at the base of lower and middle Woodford 3rd order regressive hemicycles, possible due to increasing terrestrial sediment input (Figure 28).

The Si/Al ratios variations are more complex than the Ti/Al ratios. The Si/Al ratios shows both, positive and negative correlation with the Wyche-1 GR well log (=organic content) (Figure 28). The positive correlation during the lower and middle Woodford accumulation is associated with the dominance of biogenic and authigenic quartz, related to a higher organic productivity (Figure 29), while the negative correlation in the upper Woodford was probably related to the typical dilution effect, characterized by increasing terrestrial input, including detrital quartz (Figure 30).

The biogenic quartz during the 2nd order TST deposition could have been related to a higher oceanic productivity caused by upwelling currents or continental nutrient input which contributed abundant siliceous tests and burial authigenic quartz. The diagenetic quartz could have been the result of the alteration of the original biogenic opal, derived from siliceous microfossils and also related to the intervals characterized by abundant radiolarian and silicified *Tasmanites*'s tests (Figure 29).

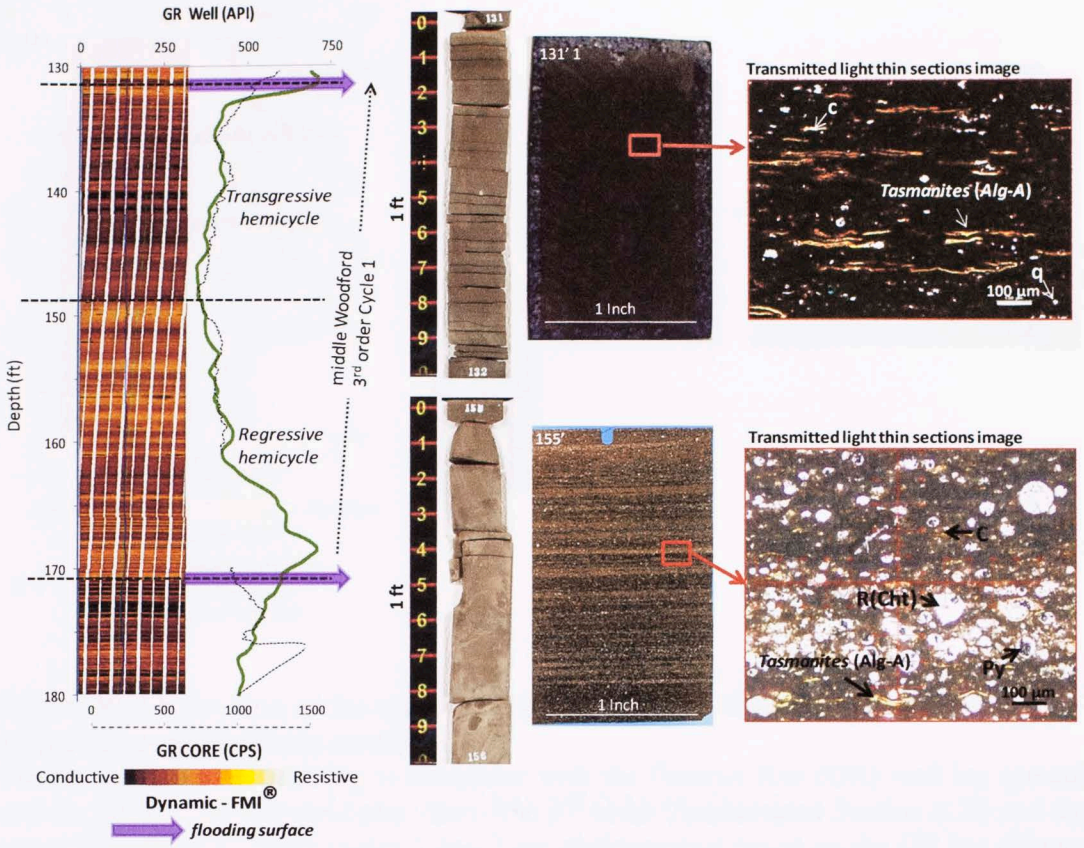

Figure 29. Illustration of the 3rd order cycles in the middle Woodford.
The middle Woodford is characterized by increasing biogenic and authigenic quartz content during 3rd order regressive hemicycle. The Dynamic-FMI® well log is compared with the Gamma Ray (GR) well log (green) and the GR core log (dashed gray line). The 3rd order cycle is differentiated based on the GR log. The FMI® is characterized by increasing lamination that is also evident in hand and thin section inspection. The thin section photo exhibits the presence of organic particles associated with acritarchs (Liptinites=*lip*) and *Tasmanites* (Alginite A or Telalginite), carbonaceous stringers (C), *Tasmanites* partially replaced with authigenic quartz, Radiolarian (R-Chert) and few detrital quartz (q) (After Sierra et al., 2010; Slatt et al., 2012).

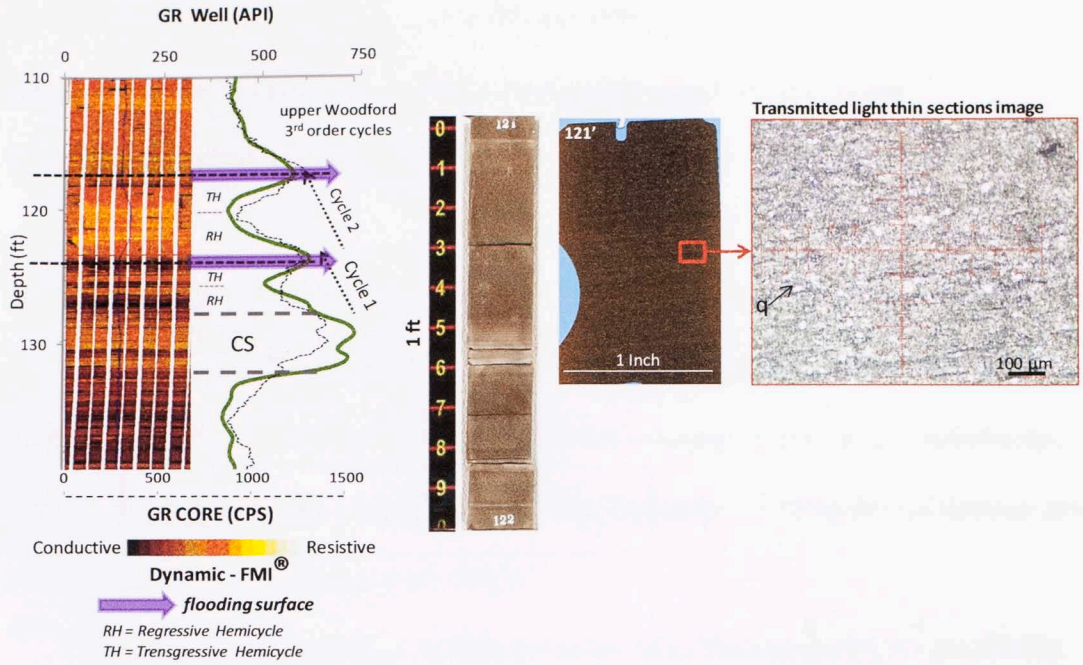

Figure 30. Illustration of the upper Woodford deposits characterized by more abundant detrital quartz content.

The Dynamic-FMI® well log is compared with the Gamma Ray (GR) well log (green) and the GR core log (dashed gray line). The 2nd order Condensated Section (CS) and the upper Woodford 3rd order cycles 1 and 2 are distinguished based on the GR log (Figure 27). The FMI® is characterized by a reduced lamination that is also evident in hand and thin section inspection (After Sierra et al., 2010; Slatt et al., 2012).

6. Discussion

6.1 The Woodford Shale Organic-Rich lithofacies and Late Devonian Transgressive-Regressive Cycles

The phenomena known as eutrophication occurs when marine ecosystems experience an excess of nutrients that stimulates the excessive growth of primary specialist species ("k- species"), which reap the nutrient benefits and increase in abundance (sometimes sizes) with respect to other generalist (r-species) organisms, creating anoxic/dysoxic sea bottom conditions (e.g.Passey et al., 2010).

Particularly two oceanic circulation models have been proposed for generating eutrophication related to anoxic/dysoxic bottom waters, responsible for triggering "black shale" facies in the Woodford Shale:

The first model is related to upwelling currents (e.g.Heckel, 1977; Parrish, 1982; Comer, 1989; 1992; Roberts and Mitterrer, 1992). The upwelling model proposes that cold, deep, oxygen-poor and phosphate-rich water from the southwestern ocean was drawn along the bottom through basins of northwest Texas and eventually upwelled in the eastern midcontinent region.

This upwelling scenario for the Woodford black shales seems to have three arguments against it (Kirkland et al., 1992): First, the location of Woodford Shale seas with respect to the paleo-equator (Miller and Kent, 1986) was untenable for an equatorial upwelling scenario (Figure 31). Second, the apparent relatively shallow condition associated with the Woodford black shales would have disallowed that major ocean current systems transferred large volumes of deep water to relatively shallower

shelf seas (Conant and Swanson, 1961; Shaw, 1964; Hallam, 1981; Kirkland et al., 1992). Third, the phosphate-rich strata which are commonly cited as evidence of upwelling are abundant in the upper Woodford, but not in the middle Woodford, where the most organic rich (anoxic/dysoxic) lithofacies are located (Figure 27). Phosphate nodules in the upper Woodford do not appear to have been triggered by upwelling currents (Kirkland et al., 1992), and in many cases, phosphorites are clearly not reliable indicators of upwelling (O'Brien and Veeh, 1983).

The second oceanic circulation model that has been proposed for generating eutrophication is associated with a epicontinental or eperic stagnant sea (e.g. Hallam, 1967; Witzke, 1987; Barron and Ettensohn, 1981; Kirkland et al., 1992). The stagnant (quasi-estuarine) circulation model postulates that the phytoplankton productivity was appreciably increased due to seasonal continental nutrient input, during a time when a wide continental shelf extension was covered by relatively shallow (< 600 m) seas (Figure 32).

Corg content and Ti/Al ratios indicate that nutrients related to terrestrial weathering may have contributed to enhanced marine productivity, in some "black" shale units such as the New Albany (Huron Shale Member) and the Marcellus Shale (e.g.Rimmer et al., 2004; Lash and Blood, 2011). The freshwater runoff for the northeastern United States during Devonian time has been related to fresher and lighter surface water flows coming from the Late Paleozoic Acadian mountains (e.g.Lash and Engelder, 2011). However, the south central Oklahoma paleoceanographic setting was different in comparison to the Appalachian Basin. Principally the Paleozoic Acadian mountains were presumably absent southward and geochemical analysis suggests a

moderate degree of water circulation (Algeo et al., 2007), possibly related with the presence of sill(s) or barrier(s) (Figure 32).

Some Woodford Shale thickness maps suggest that the Arbuckle Mountains were a paleo-high or barrier because the Woodford tends to be thinner and the Misener sandstone is absent (Amsden, 1980). Additionally, Von Almen (1970) mentioned previously that some acritarch species with complex processes or membranes (which are often associated with eutrophication), were more abundant in sediments deposited where spores occur and decreased where spores are very scarce. This observation was not confirmed in this work, but the correlation between the T-R cycles defined by Johnson et al.(1985) and the Wyche-1 well T-R cycles suggests that changes in the continental nutrient input could have influenced the accumulation of the organic-rich deposits more than upwelling currents. Upwelling currents are mainly controlled by oceanographic/atmospheric processes that in principle are not directly affected by variations in the sea (base) level and/or associated with variation in the Ti/Al ratio.

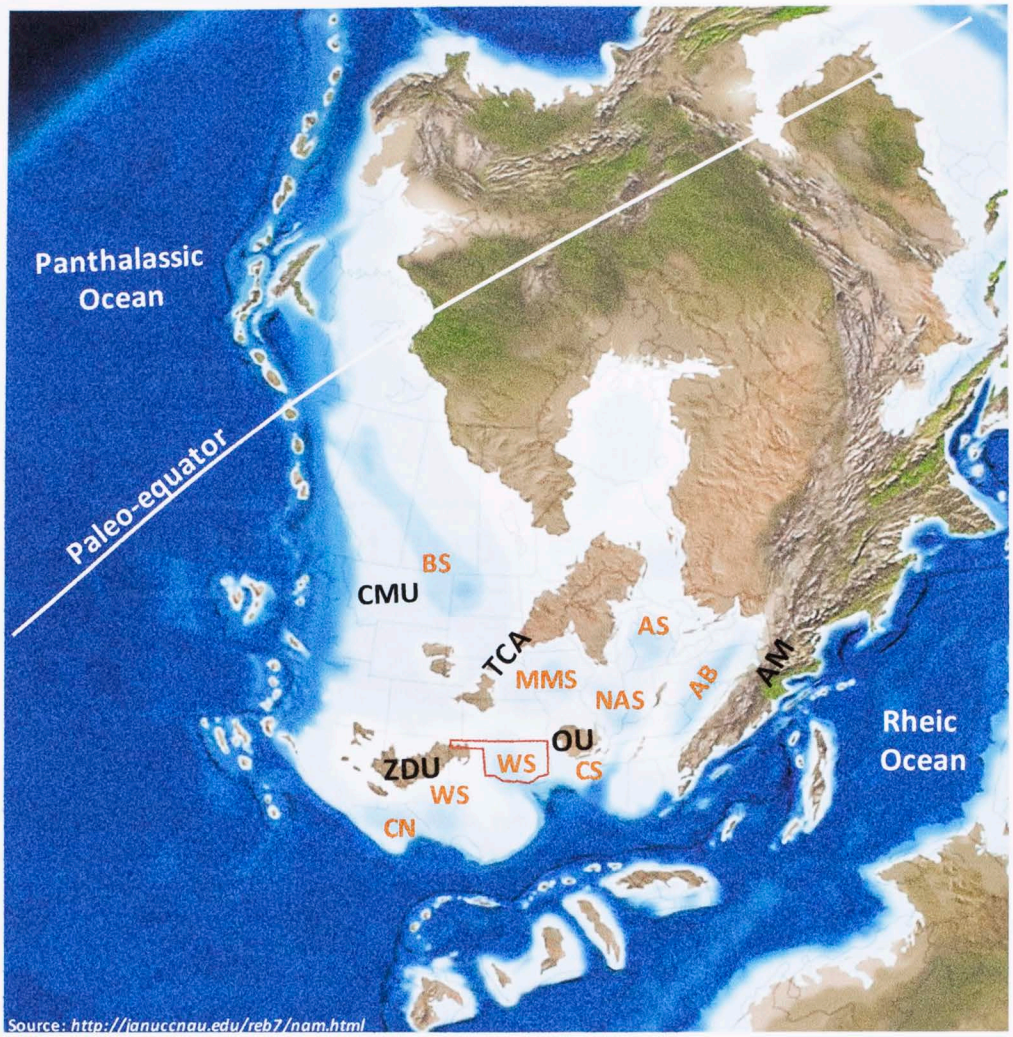

Figure 31. Late Devonian paleogeography of North America.
Paleo-equator after Miller and Kent, 1986. Oklahoma state boundaries highlighted in red color. Geographic abbreviations: AM = Acadian Mountains, TCA = Trans-Continental Arch, CMU= Central Montana Uplift, ZDU =Zuni-Defiance Uplift, OU = Ozark Uplift, BS = Bakken Shale, AS = Antrim Shale, AB = Appalachian Basin, NAS = New Albany Shale, NMS = Maple Mill Shale, CS = Chattanouga Shale, WS = Woodford Shale, CN = Caballos Novaculite. (Modified from Algeo et al., 2007).

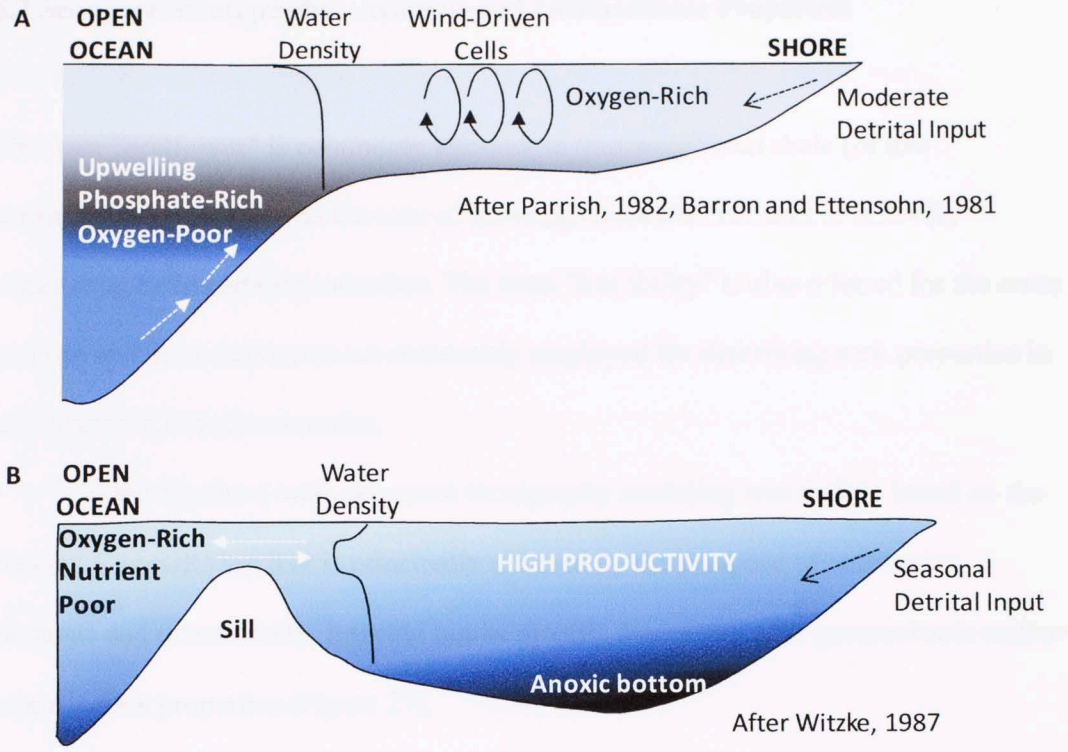

Figure 32. Oceanic circulation models for generating eutrophication
a) Upwelling model for triggering Late Devonian anoxic black shales. (After Barron and Ettensohn, 1981; Parrish, 1982). b) Stagnant (low density quasi-estuarine) circulation model for Late Devonian anoxic shales (After Witzke, 1987).

6.2 Sequence Stratigraphy, Acoustic and Geomechanic Properties

The term "brittleness" is commonly referred, in unconventional shale (or low permeability) reservoirs, as the ease of inducing hydraulic fractures in rocks for stimulating hydrocarbon production. The term "fracability" is also referred for the same purpose and these two terms are commonly employed for describing rock properties in unconventional shale reservoirs.

In the Wyche-1 well, sequence stratigraphy modeling was mainly based on the Gamma Ray (GR) log that is principally affected by the presence of radioactive elements and theoretically, it would not be directly associated with geomechanic and/or acoustic rock properties (Figure 27).

However, a higher organic content can affect fracture lengths as a consequence of the inverse proportional relation between elastic properties and organic (kerogen) content (Sierra et al., 2010; Slatt and Abousleiman, 2011; Tran et al., 2012). In fact, the sequence stratigraphy model from the Wyche-1 well seems to predict correctly the Woodford Shale intervals associated with the highest "brittleness". These potential intervals for "fracking" are related to geomechanic and acoustic properties, such as: high brittle index, high acoustic impedance, high Young's modulus, low Poisson's ratio and high geomechanic anisotropy.

Acoustic Impedance

Acoustic impedance (AI) is the product of the rock density and (P-wave) velocity (Veeken et al, 2007). AI is normally a function of the rock matrix, lithology, porosity

and fluid content. The differences in acoustic impedance in shales are related to the rock properties that affect both the "fracability" and the hydrocarbon production in unconventional reservoirs (e.g.Rich and Ammerman, 2010).

Rock geomechanic properties directly related to "fracability" can be found by inverting pre-stack or post-stack seismic data (e.g. Refunjol et al., 2011; Harris et al., 2011). Also, seismic inversion coupled with amplitude variations with offset (AVO effects) has the ability to solve parameters such as lambda-rho and mu-rho, which are directly connected to the brittleness of the rock (Perez, 2012).

The acoustic impedance for the Wyche-1 well was calculated from the Sonic (DT) and Density (RHOB) logs, using a 30 Hz Ricker Wavelet and the Petrel® software (Figure 33). The highest acoustic impedance values correspond with the 3rd order regressive hemicycles (Figure 27). The lowest acoustic impedance correspond with the intervals with the higher (GR-log) organic content (purple areas) and the highest acoustic impedance are related also to the silica-rich, brittle intervals (Figure 33).

The 'brittleness index' (BI) was based upon mineralogy composition from the ECS log and TOC were estimated from GR log (Figure 9). The assumption behind the brittleness index is that quartz and sometimes dolomite and/or calcite rich rocks will be more brittle than clay and organic-rich rocks (Figure 33 and 34).

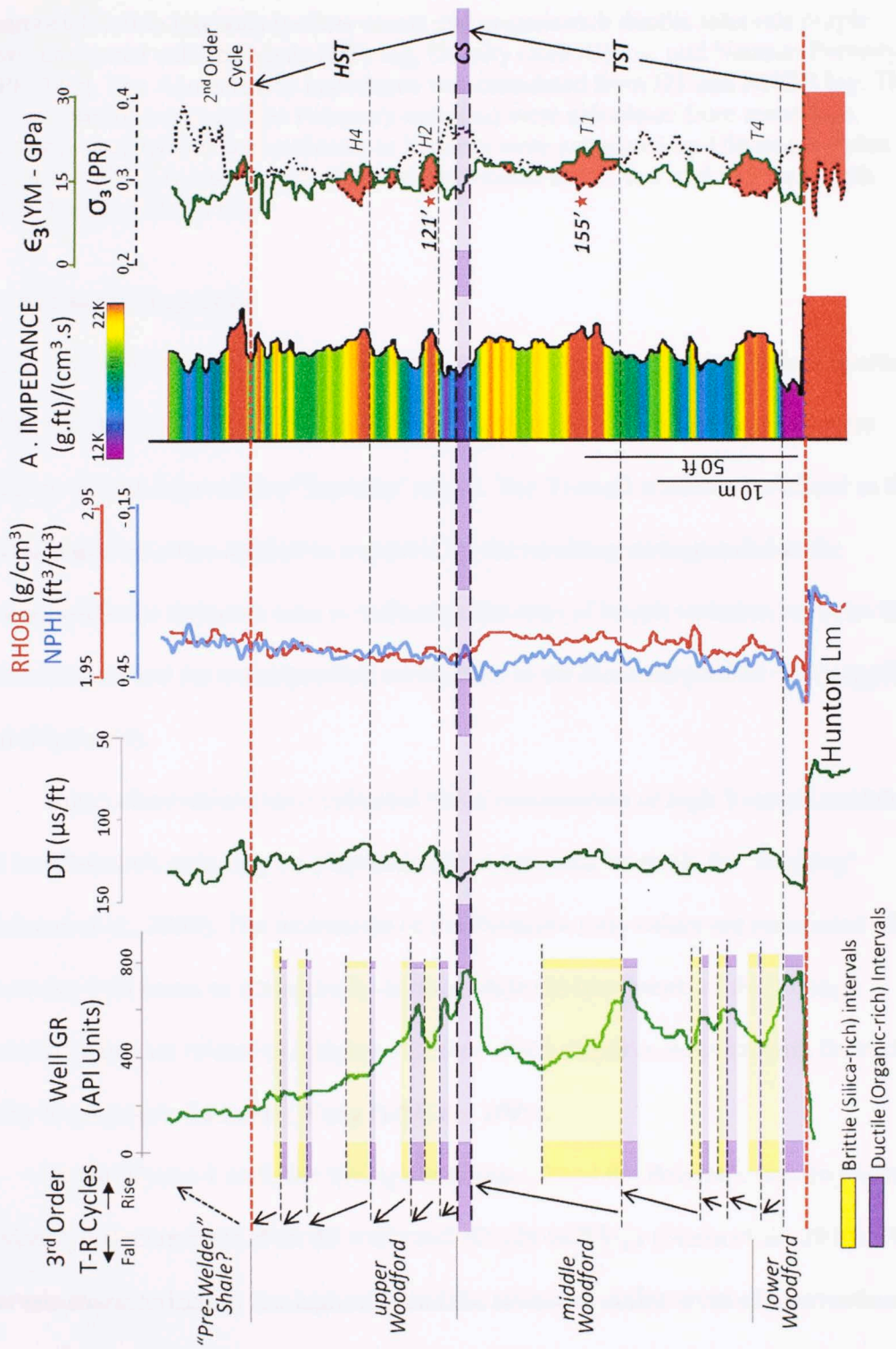

Figure 33. Sequence Stratigraphy, Acoustic and Geomechanic Properties.

Quartz-rich brittle intervals (yellow areas) and organic-rich ductile intervals purple areas) compared with the Sonic (DT) log, Density (RHOB) log, and Neutron Porosity (NPHI) log. The Acoustic (A) Impedance was calculated from DT and RHOB log. The Young's modulus (ϵ_3) and the Poisson's ratio (σ_3) were calculated from sonic logs. Properties parallel and perpendicular to bedding were calculated by Ultrasonic Pulse Velocities (UPV) in two samples (Red Stars) located at 121 feet and 155 feet depth (After, Sierra et al., 2010).

Geomechanic Properties

The Young's modulus (ϵ) and the Poisson's ratio (σ) are geomechanic elastic properties and two of the most important parameters in engineering well design, including the selection of rock intervals for "fracking" stages. The Young's modulus is defined as the ratio of a tension stress applied to a material to the resulting strain parallel to the tension, while the Poisson's ratio is defined as the ratio of length variation between the rock extension and the corresponding contraction in the direction parallel to the applied load (Figure 34).

Some observations have indicated that a combination of high Young's modulus and low Poisson's ratio may be diagnostic of the best rock intervals for "fracking" (Rickman et al., 2008). The increments of the Poisson's ratio values are associated with decreasing brittleness or increasingly ductile, while the increments of the Young's modulus values are related to a higher stiffness which would correspond with the rock ability to propagate fractures (Wang and Gale, 2009).

In the Wyche-1 well, the Young's modulus (ϵ) and the Poisson's ratio (σ) were previously calculated based on the sonic and density well logs (Sierra et al., 2010). The intervals characterized by the highest ϵ_3 and the lowest σ_3 define areas of intersection crossover, which roughly correspond with the brittle regressive intervals, predicted by the sequence stratigraphy modeling (Figure 33).

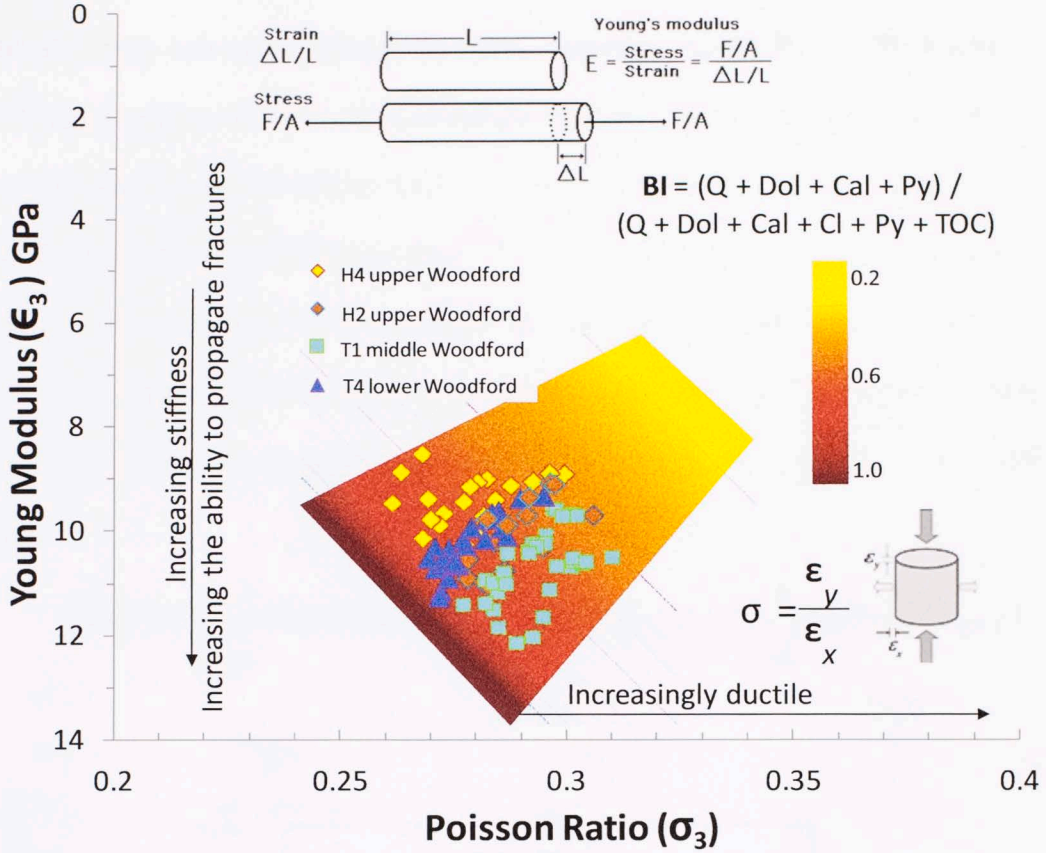

Figure 34. Young's modulus (ϵ3) and Poisson's ratio (σ3) calculated for only those crossover intervals, characterized by the highest ϵ3 and the lowest σ3 from the Wyche-1 well.
The yellow and orange colors represent the brittle intervals associated with the upper Woodford regressive hemicycles and the blue color represent the brittle intervals associated with the lower and middle Woodford regressive hemicycles.
BI = Brittle Index; Q = quartz; Dol = dolomite; Cal = Calcite; Py = Pyrite; Cl = Clay minerals; TOC = Total Organic Carbon

Geomechanical and mineralogical properties are related (Figure 34). Rocks with a relatively large numerical value of Poisson's ratio and small Young's modulus tend to have a low brittleness index and are thus ductile. Rocks with a small Poisson's ratio and a large Young's modulus tend to have a higher brittleness index and are thus relatively more brittle.

Anisotropy

The anisotropy was not included in the elastic properties calculated from the Wyche-1 well logs (ϵ_3 and σ_3) and it is assumed that the Woodford Shale mechanical properties are isotropic. But, the Woodfords Shale is evidently anisotropic (Figure 29 and 30). The middle and lower Woodford brittle (biogenic quartz-rich) intervals are characterized by more abundant laminations in comparison with the upper Woodford brittle (detrital quartz-rich) strata (Figure 29 and 30). These differences are evident on Micro-resistivity (FMI®) logs, hand and thin section inspection and geomechanic properties also (Figure 35).

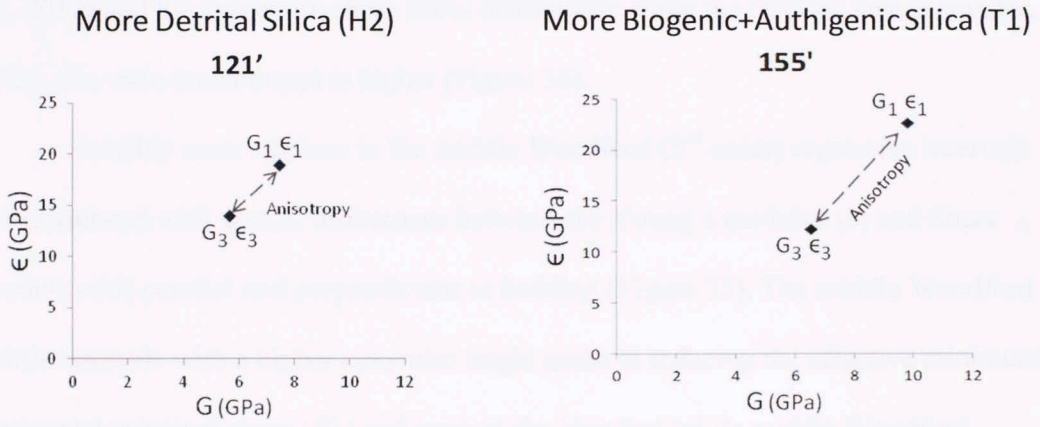

Figure 35. Young's modulus (ϵ) and Shear modulus (G) calculated by Ultrasonic Pulse Velocities (UPV), parallel (1) and perpendicular to bedding (3).
These two samples were located in 3rd order regressive hemicycles in the upper Woodford (121ft) and middle Woodford (155 ft). GPa = Giga Pascal. UPV values from Sierra et al.(2010).

In geomechanic modeling, an existing fracture opens and propagates at the fracture tip, if the fracturing fluid creates a tensile stress that exceeds the effective minimum horizontal principal stress (S'_h). The routine approach for calculating the S'_h assuming a rock with vertical transverse isotropy (VTI) and only affected by

overburden stress (non tectonically active areas), was described previously by Amadei et al., (1987) as:

$$S'_h = \frac{\epsilon_1}{\epsilon_3} \frac{\sigma_3}{1-\sigma_1} (S_v - \alpha_3 P)$$

ϵ, σ, α, S_v, P are respectively the Young's modulus, Poisson's ratio, Biot's pore pressure coefficient, overburden stress and pore pressure; the subscript "1" and "3" represent properties in directions parallel and perpendicular to bedding planes.

The Young's modulus value measured parallel to bedding (ϵ_1) is apparently the most sensitive poro-elastic parameter to the variations in the horizontal stress (Tran et al., 2012) and the maximum shear stress distribution along the fracture face is smaller, if the ϵ_1/ϵ_3 ratio (anisotropy) is higher (Figure 36).

Possibly more laminae in the middle Woodford (3rd order) regressive intervals are associated with greater differences between the Young's modulus (ϵ) and Shear modulus (G) parallel and perpendicular to bedding (Figure 35). The middle Woodford brittle intervals with a higher ϵ_1/ϵ_3 ratio might assist in reducing the effective minimum horizontal principal stress (S'_h) and support the idea that brittle middle Woodford intervals are better than brittle upper and lower Woodford intervals for "Fracking", because more abundant brittle biogenic quartz rich laminae may act as planes of weakness during hydraulic fracturing processes.

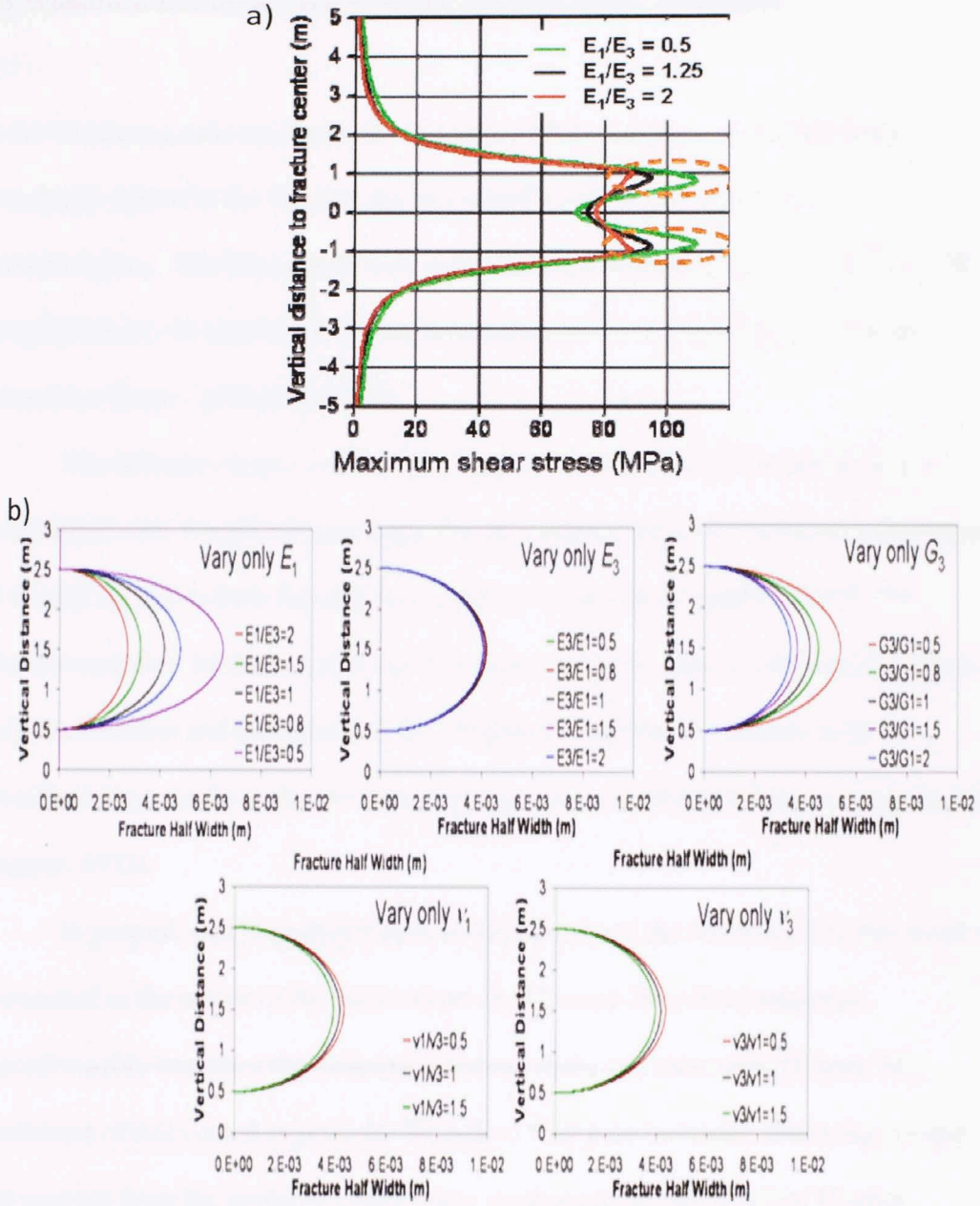

Figure 36. Sensitivity models for fracture propagation.
a) Sensitivity model for the variation of the maximum shear stress (Mpa = Mega Pascal) in the fracture face (x-axis), related to the Young's modulus in direction parallel (E_1) and perpendicular (E_3) to bedding planes. b) Sensitivity model for the variation of the fracture width, related to the changes in the elastic properties in directions parallel and perpendicular to bedding. E=Young's modulus; G= Shear's modulus; v= Poisson's ratio (Tran et al., 2012).

6.3 Woodford thickness changes in the Arkoma Basin, Oklahoma

In the Oklahoma Arkoma Basin, the Woodford Shale variations in thickness are principally related to the fact that the Woodford's bottom and top limits are unconformities. The Woodford Shale in the Arkoma Basin is generally 100 feet (~30 m) to 200 feet (~61 m) thick but thins to less than 50 feet (~16 m) thick northeast toward the Ozark Uplift (Figure 37).

The Misener clearly overlies the pre-Woodford unconformity and locally is interbedded with Woodford-type shale. For that reason, these two units are believed to be closely related in their depositional history (Amsden and Klapper, 1972). The Misener conodont faunas range in age from late Middle to Late Devonian (Givetian to early Famennian) and indicates that the Misener is correlative with part of the Woodford Shale in the region of Arbuckle Mountains southern Oklahoma (Amsden and Klapper, 1972).

In general , the Woodford Shale is thicker toward the southwest but this trend is interrupted in the center of the basin where the Misener-Woodford sequence unconformably truncates the underlying Sylvan shale and older units (Figure 38). Southwest of this central region, the Woodford thickness increases, following a trend that extends from the northern Coal County northward through much of Hughes County, where most of the horizontal Woodford wells have been drilled (Figure 2). There, the Woodford Shale ranges from 7,000 feet (~2130 m) to 10,500 feet (~3200 m) deep and it has thickness between 100 feet (~30 m) to 200 feet (~61 m) (Amsden, 1980, Panel 3).

In the eastern Arbuckle Mountains, the Woodford is thinner (< 100 ft; ~30 m) and the Misener sandstones are not reported (Amsden and Klapper, 1972), may be related to the absence of any substantial local source for such material nearby (Amsden, 1960, p. 139-140).

Thermal maturity is another clear control on the Woodford Shale play distribution. The Woodford Shale producing wells tend to be concentrated in areas where the percentages of vitrinite reflectance(Ro) are between 1% and 3% (Cardott, 2012) and condensate and liquid production is mainly related to the Ro 1.4% contour, where typically isotopic inversion phenomena (e.g. Rodriguez and Slatt, 2012) could be taking place (Figure 2).

Finally, in addition to geological factors, many variables may affect the hydrocarbon production from horizontal Woodford Shale wells in the Arkoma Basin. Unfortunately, only a few are quantified or reported by operating companies (Andrews, 2009). These variables may include the amount and type of fluid and proppant used in fracturing, number and length of stages, and completion techniques.

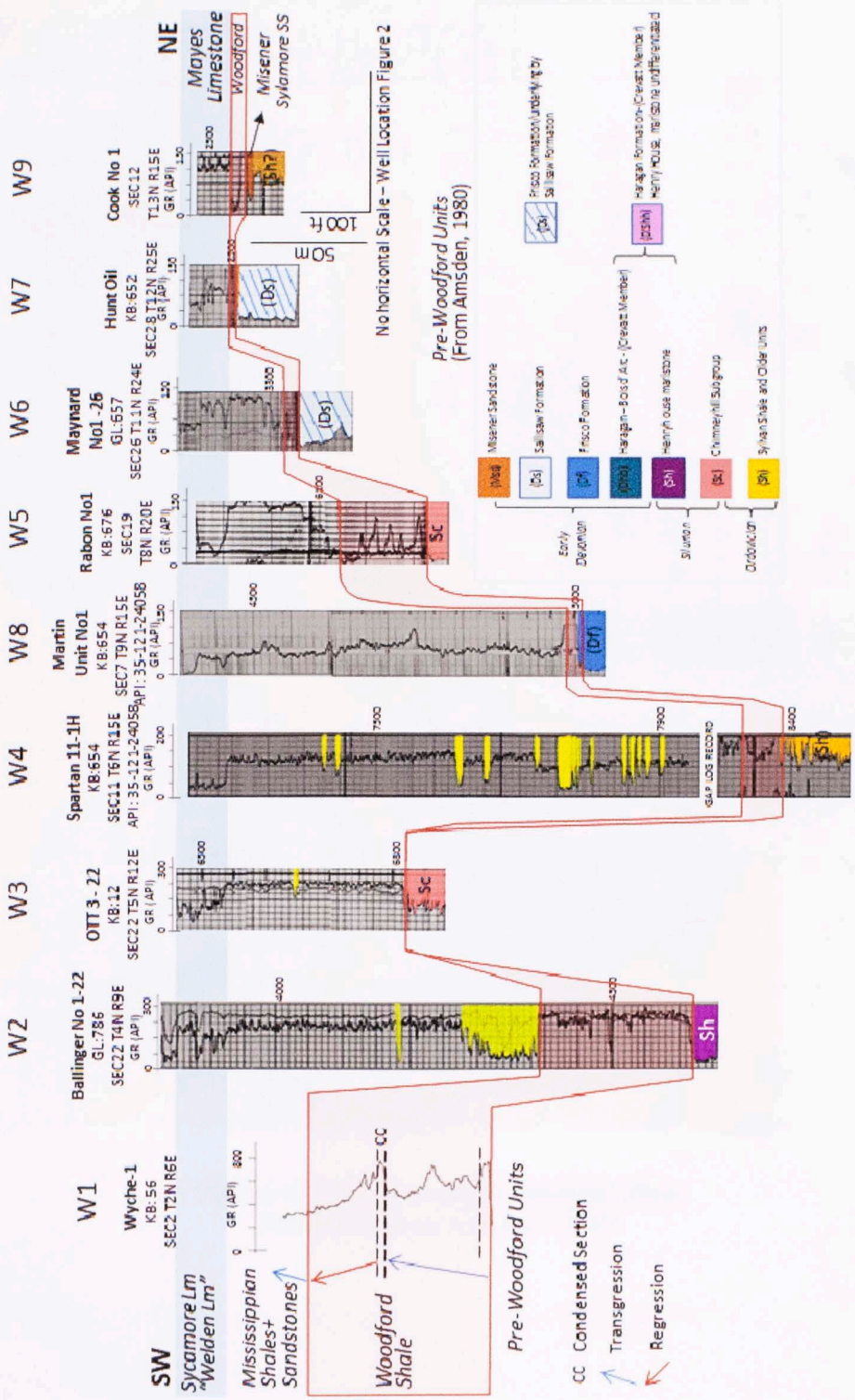

Figure 37. Regional Cross-Section flattened to the Mississippian limestones base.

Cross Section location in Figure 38

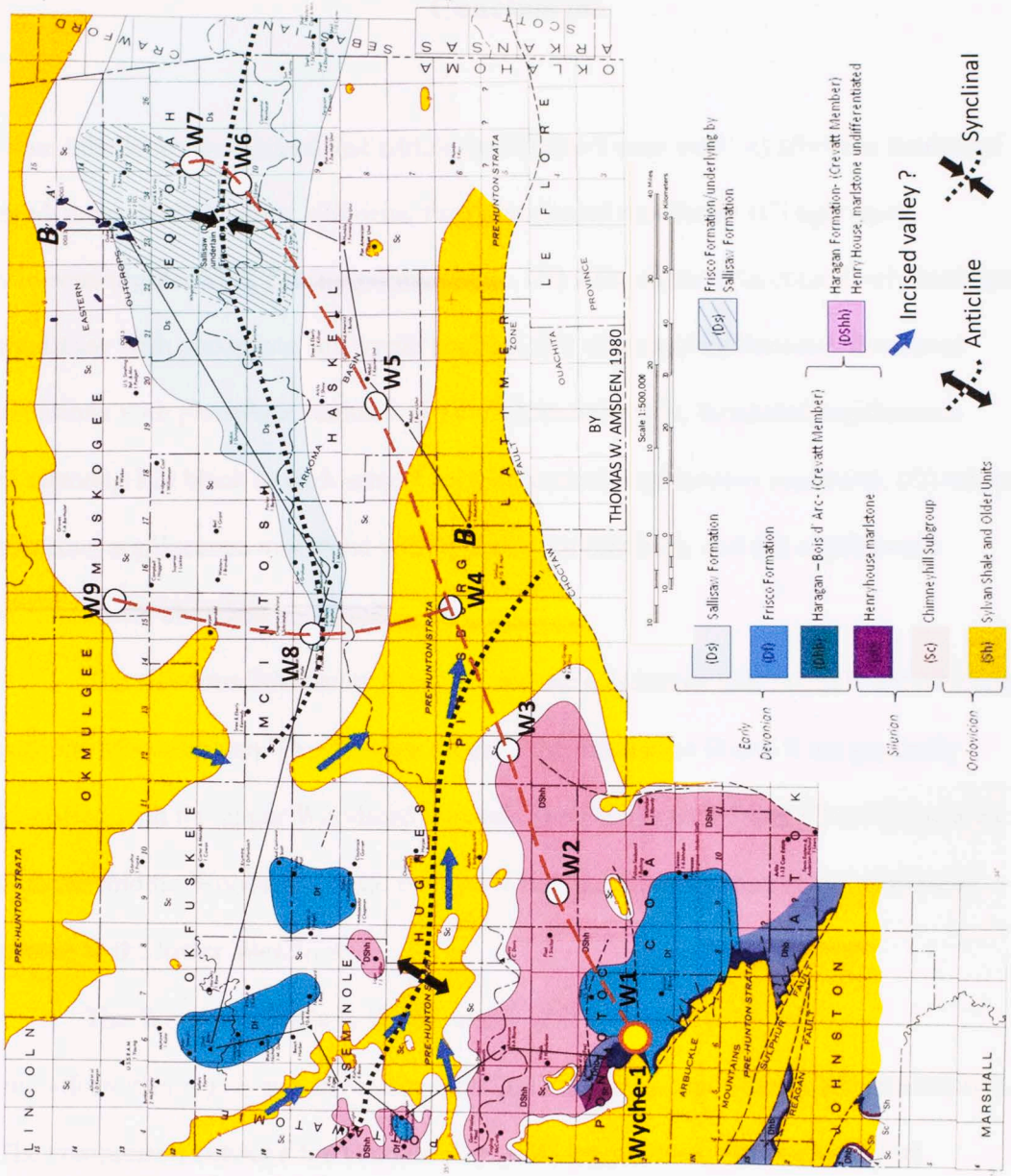

Figure 38. Pre-Woodford Geologic Map.
(Modified from Amsden, 1980)

Conclusions

Nine lithofacies were identified within the Wyche-1 core well: A) siliceous laminated mudstone, (B) light-gray, siliceous, finely laminated mudstone, (C) light-gray, siliceous/argillaceous, calcareous mudstone, (D) siliceous/argillaceous, finely laminated mudstone with phosphate and pyrite nodules, (E) siliceous/argillaceous, laminated mudstone with phosphate nodules, (F1) black to dark gray, laminated argillaceous mudstone, (F2) black to dark gray, finely laminated, argillaceous mudstone, (G) mixed siliceous/argillaceous mudstone with thin clay laminations, and (H) argillaceous siltstone with abundant angular detrital quartz.

The siliceous lithofacies A and B, and the calcareous lithofacies C are associated with the Mississippian "Pre-Welden Shale". The lithofacies D and E are generally identified with the upper Woodford interval. The lithofacies F1 and F2 are associated with the middle Woodford, while the quartz rich lithofacies G and H are commonly related to the lower Woodford.

The Woodford Shale in the Wyche-1 well is present between two unconformities which are associated with 2nd order sequence stratigraphy boundaries. The comparison between the Gamma Ray (GR) log patterns, the Palynological assemblages (Pollen Index) and the Ti/Al and Si/Al ratios illustrate that the lower and middle Woodford correspond to 2nd order Trangressive System Tract (TST), with five 3rd order cycles, and the upper Woodford to 2nd order Highstand System Tract (HST) deposits, with six 3rd order cycles.

The middle Woodford interval show a positive correlation between GR (Total Organic Carbon = TOC content) log and Si/Al ratios, while the lower and upper Woodford intervals show a negative correlation between the GR (TOC content) log and Si/Al ratios. The middle Woodford more brittle intervals are associated with 3rd order regressive hemicycles, with more biogenic and authigenic quartz, because of increased biological productivity and the upper and lower Woodford more brittle intervals are associated with 3rd order regressive hemicycles, but related to increases in detrital quartz.

In general, the 3rd order regressive hemicycles were characterized by high acoustic impedance, high Young's modulus and low Poisson's ratio. But the middle Woodford intervals are more anisotropic than the lower and upper Woodford, because of more laminations.

Finally, thermal maturity is a clear control in the Woodford Shale play distribution in the Arkoma Basin. In addition, the unconformities located above and below the Woodford deposits are clearly affecting the Woodford Shale thickness and potentially the areal distribution of the Woodford Shale play in the Arkoma Basin of Oklahoma.

References

Abouelresh, M.O., and R.M. Slatt, 2012, Lithofacies and sequence stratigraphy of the Barnett Shale in east-central Fort Worth Basin, Texas: AAPG Bulletin, v. 96, p. 1-22.

Abousleiman, Y., M. Tran, S. Hoang, C. Bobko, A. Ortega, and F. J. Ulm, 2007, Geomechanics field and lab characterization of Woodford Shale: The next gas play: Society of Petroleum Engineers Paper 110120, Society of Petroleum Engineers Annual Technical Conference Exhibition, Anaheim, California, November 11–14, 14 p.

Abousleiman, Y., M. Tran, S. Hoang, J. A. Ortega, and F. J. Ulm, 2009, GeoMechanics field characterization of the two prolific U.S. mid-west gas plays with advanced wireline logging tools: Society of Petroleum Engineers Paper 124428, Society of Petroleum Engineers Annual Technical Conference Exhibition, New Orleans, Louisiana, October 4–7. 19 p.

Algeo, T. J., T. W. Lyons, R. C. Blakey, and D. J. Over, 2007, Hydrographic conditions of the Devono-Carboniferous North American Seaway inferred from sedimentary Mo-TOC relationships: Palaeogeography Palaeoclimatology Palaeoecology, v. 256, p. 204-230.

Amadei, B., W. Z. Savage, and H. S. Swolfs, 1987, Gravitational stresses in anisotropic rock masses: Int. J. Rock Mech. Min. Sci. & Geomech. Abstract. 24, p. 5-14.

Amsden, T. W., 1960, Hunton stratigraphy, part 6 of stratigraphy and paleontology of the Hunton Group in the Arbuckle Mountain region: Oklahoma Geological Survey Bulletin, v. 84, 311 p.

Amsden, T. W., 1980, Hunton Group (Late Ordovician, Silurian, and Early Devonian) in the Arkoma basin of Oklahoma: Oklahoma Geological Survey Bulletin, v. 129, 136 p.

Amsden, T.W., and G. Klapper, 1972, Misener Sandstone (Middle-Upper Devonian), north-central Oklahoma: AAPG Bulletin, v. 56, p. 2323-2334.

Andrews, R. D., 2009, Production decline curves and payout thresholds of horizontal Woodford well in the Arkoma Basin, Oklahoma: Shale Shaker, v. 60, p. 103-112.

Barrick, J.E., J. N. Haywa-Branch, and D.J. Over, 1990, Stop 6: Woodford Shale (Late Devonian-Early Mississippian), pre-Weldon Shale, Weldon Limestone, and basal Caney Shale (Mississippian); Hass G section, *in* S.M. Ritter, eds., Early and middle Paleozoic conodont biostratigraphy of the Arbuckle Mountains, southern Oklahoma: OGS Guidebook 27, p. 23-25.

Barron, L.S., and F.R., Ettensohn, 1981, Paleoecology of the Devonian-Mississippian black shale sequence in eastern Kentucky with an atlas of some common fossils: Springfield, Technical Information Center, U.S. Department of Energy, DOE/ ET/12040-151, 75 p.

Bohacs, K.M., 1990, Sequence Stratigraphy of the Monterey Formation, Santa Barbara County: Integration of Physical, Chemical, and Biofacies Data from Outcrop and subsurface: SEPM, Core Workshop 14, San Francisco, Ca. p. 139–200.

Bohacs, K.M., G. J., Grawbowski, A. R., Carroll, P. J., Mankeiwitz, K. J., Miskell-Gerhardt, J. R., Schwalbach, M. B., Wegner, and J. A. Simo, 2005, Production, Destruction, and Dilution – the Many Paths to Source-Rock Development: SEPM Special Publication v. 82, p. 61-101.

Bohacs, K., and J., Schwalbach, 1992, Sequence stratigraphy of fine-grained rocks with special reference to the Monterey Formation, *in* J. Schwalbach, and K. Bohacs, eds., Sequence Stratigraphy in Fine-Grained Rocks: Examples from the Monterey Formation, SEPM Pacific Section, v. 70, p 7-19.

Branson, C. C., 1957, Some regional features of Mississippian and Early Pennsylvanian rocks in the Mid-Continent: Abilene and Fort Worth Geol. Soc. Joint Field Trip Guide Book, p. 79-83.

Buckner, T. N., R. M. Slatt, B. Coffey, and R. J. Davis, 2009, Stratigraphy of the Woodford Shale from behind-outcrop drilling, logging, and coring: AAPG Search and Discovery article 50147 < http://www.searchanddiscovery.net/documents/2009/50147buckner/ndx_buckner.html > (Accessed September 10, 2012).

Cardott, B.J., 2005, Overview of unconventional energy resources of Oklahoma, *in* B.J. Cardott, eds., Unconventional Energy Resources in the Southern Midcontinent, 2004 Symposium: Oklahoma Geological Survey Circular, v. 110, p. 7–18.

Cardott, B.J., 2007, Overview of Woodford gas-shale play in Oklahoma: OGS, Woodford Gas Shale Conference, May 23, 2007, PowerPoint presentation. < http://www.ogs.ou.edu/pdf/WoodfordOverview.pdf. > (Accessed September 10, 2012).

Cardott, B.J., 2012, Thermal maturity of Woodford Shale gas and oil plays, Oklahoma, USA: Journal of Coal Geology, v. 103, p. 109-119.

Cardott, B.J., and J.R. Chaplin, 1993, Guidebook for Selected Stops in the Western Arbuckle Mountains, Southern Oklahoma: Oklahoma Geological Survey Special Publication, v.93, no. 3. 55 p.

Catuneanu, O., V. Abreu, J.P. Bhattacharya, M.D. Blum, R.W. Dalrymple, P.G. Eriksson, C.R. Fielding, W.L. Fisher, W.E. Galloway, M.R. Gibling, K.A. Giles, J.M. Holbrook, R. Jordan, C.G.St.C. Kendall, B. Macurda, O.J. Martinsen, A.D. Miall, J.E. Neal, D. Nummedal, L. Pomar, H.W. Posamentier, B.R. Pratt, J.F. Sarg, K.W. Shanley, R.J. Steel, A. Strasser, M.E. Tucker, and C. Winker, 2009, Towards the standardization of sequence stratigraphy: Earth-Science Reviews, v. 92, p. 1-33.

Comer, J.B., 1989, Depositional model for Upper Devonian black shale (Woodford Formation) in Permian basin, West Texas and southeastern New Mexico [Abstract]: American Association of Petroleum Geologists Bulletin, v. 73, p. 346

Comer, J.B., 1992, Organic Geochemistry and Paleogeography of Upper Devonian Formations in Oklahoma and Northwestern Arkansas, *in* K.S. Johnson, and B.J. Cardott, eds., Source Rocks in the Southern Midcontinent, 1990 Symposium: OGS Circular, v. 93, p. 70-93.

Conant, L.C., and V. E. Swanson, 1961, Chattanooga Shale and related rocks of central Tennessee and nearby areas: U.S. Geological Survey Professional Paper 357, 91 p.

Evitt, W R., 1963a. A discussion and proposals concerning fossil dinoflagellates, hystrichospheres, and acritarchs: I. Proc. Natl. Acad. Sci., Washington, vol. 49 p. 158-164.

Evitt, W.R., 1963b. A discussion and proposals concerning fossil dinoflagellates, hystrichospheres, and acritarchs: II. Proceedings of the National Academy of Sciences of the United States of America, Washington, vol. 49, p. 298-302.

Gradstein, F., J. Ogg., and A. Smith, 2004, A Geological Time Scale 2004: Cambridge Univ. Press., 589 p.

Grieser, B., 2011, Oklahoma Woodford Shale: Completion trends and production outcomes from three basins: Paper Society of Petroleum Engineers Paper 139813, presented at the SPE Annual Technical Conference and Exhibition, San Antonio, Texas, USA, September 24 -27 14 p.

Guy-Ohlson, D., 1988, Developmental stages in the life cycle of Mesozoic Tasmanites: Botanica Marina vol. 31, p. 447 - 456.

Hallam, A., 1967, The depth significance of shales with bituminous laminae: Marine Geology, v.5, p 481 - 493

Hallam, A., 1981, Facies interpretation in the stratigraphic record: W. H. Freeman, San Francisco, 291 p.

Harris, N. B., Miskimins, J. L., and C. A., Mnich, 2011, Mechanical Anisotropy in the Woodford Shale, Permian Basin: Origin, Magnitude, and Scale: The Leading Edge, p. 284-291.

Heckel, P. H., 1977, Origin of phosphatic black shale facies in Pennsylvanian cyclothems of Mid-Continent North America: AAPG Bulletin, v.61, p. 1045-1068.

Jacobson, S. R., 1979, Acritarchs as paleoenvironmental indicators in Middle and Upper Ordovician rocks from Kentucky, Ohio and New York: Journal of Paleontology, v. 53, p. 1197-1212.

Johnson, K. S., 2008, Geologic Historic of Oklahoma: Educational Publication, no. 9, 9 p.

Johnson, J.G., G. Klapper, and C.A. Sandberg, 1985, Devonian eustatic fluctuations in Euramerica: Geological Society of America Bulletin, v. 96, p. 567-587.

Johnson, J. G., and G. Klapper, 1992, North American midcontinent Devonian T-R cycles, *in* Chaplin, J.R., and Barrick, J. E., eds., Special papers in paleontology and stratigraphy: A tribute to Thomas W. Amsden: Oklahoma Geological Survey Bulletin 145, p. 127-135.

Johnson, K. S., and B. J. Cardott, 1992, Geologic framework and hydrocarbon source rocks of Oklahoma, *in* K. S. Johnson and B. J. Cardott, ed., Source rocks in the southern Midcontinent, 1990 symposium: OGS Circular v. 93, p. 21–37.

Kirkland, D. W., R. E. Denison, D. M. Summers, and J. R. Gormly, 1992, Geology and organic geochemistry of the Woodford Shale in the Criner Hills and western Arbuckle Mountains, Oklahoma, *in* K. S. Johnson and B. J. Cardott, eds., Source rocks in the southern mid-continent: 1990 Symposium: OGS Circular v. 93, p. 38–69.

Lash, G. G., and R. Blood, 2011, Chemostratigraphic trends of the Middle Devonian Marcellus Shale, Appalachian Basin: Preliminary Observation: AAPG Search and Discovery Article #80198 (2011) < http://www.searchanddiscovery.com/documents/2011/80198lash/ndx_lash.pdf > (Accessed September 10, 2012).

Lash, G. G., and T. Engelder, 2011, Thickness trends and sequence stratigraphy of the Middle Devonian Marcellus Formation, Applachian basin: Implications for Acadian foreland basin evolution: AAPG Bulletin, v. 95, no. 1, p. 61 - 103.

McGhee, G.R.J., 1996, The Late Devonian mass extinction - the Frasnian/Famennian crisis. Critical Moments in Paleobiology and Earth History Series: Columbia University Press, New York, 303 p.

Miceli-Romero, A., and R. P. Philp., 2012, Organic geochemistry of the Woodford Shale, southeastern Oklahoma: How variable can shales be?. AAPG Bulletin: v. 96, no. 3, p. 493–517.

Miller, J. D., and D. V., Kent, 1986, Synfolding and prefolding magnetizations in the Upper Devonian Castkill Formation of eastern Pennsylvanian: implications for the tectonic history of Acadia: Journal of Geophysical Research, v. 91, p. 12791-12803.

Molyneux, S.G., A.L., Herisse and R. Wicander, 1996, Paleozoic phytoplankton, *in* J. Jansonius, and D. C. Gregor, eds., Palynology: Principles and Applications. American Association of Stratigraphic Palynologists Foundation, v. 2, p. 493-529.

Northcutt, R.A., and J.A. Campbell, 1996, Geologic provinces of Oklahoma: Oklahoma City Geological Society Shale Shaker, v. 46, p. 99-103.

Northcutt, R. A., K. S. Johnson, and G. C. Hinshaw, 2001, Geology and petroleum reservoirs in Silurian, Devonian, and Mississippian rocks in Oklahoma, *in* K. S.

Johnson, ed., Silurian, Devonian, and Mississippian geology and petroleum in the southern mid-continent: 1999 Symposium: OGS Circular v. 105, p. 1–29.

O'Brien, N. R., and R. M. Slatt, 1990, Argillaceous rock atlas: NY, Springer-Verlag, 141 p.

O'Brien, G. W., and H. H. Veeh, 1983. Are phosphorites reliable indicators of upwelling? *in* Thiede, J., and E., Suess, eds., Coastal Upwelling, Its Sedimentary Record, Part A. New York (Plenum Press), p. 399-420.

Over, D.J., 1990, Conodont biostratigraphy of the Woodford Shale (Late Devonian-Early Carboniferous) in the Arbuckle Mountains, south-central Oklahoma: Texas Tech University unpublished Ph.D. dissertation, 174 p.

Over, D.J., 1992, Conodonts and the Devonian-Carboniferous boundary in the upper Woodford Shale, Arbuckle Mountains, south-central Oklahoma: Journal of Paleontology, v. 66, p. 293-311.

Over, D.J., and J.E. Barrick, 1990, The Devonian/Carboniferous boundary in the Woodford Shale, Lawrence uplift, south-central Oklahoma, *in* S.M. Ritter, eds., Early to middle Paleozoic conodont biostratigraphy of the Arbuckle Mountains, southern Oklahoma: OGS Guidebook 27, p. 63-73.

Over, D.J., 2002, The Frasnian/ Famennian boundary in central and eastern United States: Palaeogeography, Palaeoclimatology, Palaeoecology, v. 181, p. 153-169.

Parrish, J. T., 1982, Upwelling and petroleum source beds, with reference to Paleozoic: AAPG Bulletin, v. 66, p. 750-774.

Passey, Q. R., K. M., Bohacs, R. Esch, and S. Sinha, 2010, From oil-prone source rock to gas-producing shale reservoir – Geologic and petrophysical characterization of unconventional shale gas reservoirs, SPE 131350.

Paxton, S. T., A. Cruse, and A. Krystyniak, 2007, Fingerprints of global sea level change revealed in hydrocarbon source rock? < http://www.searchanddiscovery.net/documents/2006/06095paxton/images/paxton.pdf > (Accessed September 18, 2012).

Perez, R., 2012, Application of LMR and Clustering Analysis in Unconventional Reservoirs: Search and Discovery Article #40879 (2012) Posted February 13, 2012 < http://www.searchanddiscovery.com/documents/2012/40879perez/ndxperez.pdf > (Accessed April 6, 2013).

Portas, R., 2009, Characterization and origin of fracture patterns in the Woodford Shale in southeastern Oklahoma for application to exploration and development: Master's thesis, University of Oklahoma, Norman, Oklahoma, 113 p.

Posamentier, H. W., and G. P. Allen, 1999, Siliciclastic sequence stratigraphy: concepts and applications, Concepts in Sedimentology and Paleontology vol. 7: Society of Economic Paleontologists and Mineralogists (SEPM) 210 p.

Rich, J.P., and M. Ammerman, 2010, Unconventional geophysics for unconventional plays. SPE paper 131779, SPE Unconventional Gas Conference in Pittsburgh, Pennsylvania. 14p.

Richardson J. B., and S. M., Rasul. 1990, Palynofacies in a Late Silurian regressive sequence in the Welch Borderland and Wales: Journal of the Geological Society, London, v. 147, p. 675-686.

Rickman, R., M. Mullen, E. Petre, B. Grieser, and D. Kundert, 2008, "A Practical Use of Shale Petrophysics for Stimulation Design Optimization: All Shale Plays Are Not Clones of the Barnett Shale": SPE paper 115258, SPE Annual Technical Conference and Exhibition, 21-24 September 2008, Denver, Colorado, 14 p.

Rimmer, S. M., Thompson, J. A., Goodnight, S. A., and T. L. Robl, 2004, Multiple controls on the preservation of organic matter in Devonian-Mississippian marine black shales geochemical and petrographic evidence: Palaeogeography, Palaeoclimatology, Palaeoecology, Vol 215, p. 125– 154.

Ritter, S.M, 1990, Early and middle Paleozoic conodont biostratigraphy of the Arbuckle Mountains, southern Oklahoma: OGS Guidebook 27, 114 p.

Roberts, C. T., and R. M. Mitterrer, 1992, Laminated Black Shale-Bedded chert cyclicity in the Woodford Formation, Southern Oklahoma. *in*: Johnson, K.S., and B. J. Cardott, eds., Source Rocks in the Southern Midcontinent, 1990 Symposium: OGS Circular v. 93, p 330.

Rodriguez, N. D., and R. M. Slatt, 2012, Comparative sequence stratigraphy and organic geochemistry of gas shales: Commonality or coincidence?: Journal of Natural gas science and engineering, v. 8, p. 68 - 84.

Schieber, J., 1996, Early diagenetic silica deposition in algal cysts and spores: a source of sand in black shales?: Journal of Sedimentology Research, v. 66, p. 175– 183.

Schmitz, B., 1987, The TiO2/Al2O3 ratio in the Cenozoic Bengal abyssal fan sediments and its use as a palaeostream energy indicator: Marine Geology v. 76, p. 195 – 206.

Shaw, A B., 1964, Time in stratigraphy: McGraw-Hill, New York, 365 p.

Sierra, R., M. H. Tran, Y. N. Abousleiman, and R. M. Slatt, 2010, Woodford Shale mechanical properties and impacts of lithofacies: 44th U.S. Rock Mechanics Symposium, Salt Lake City (ARMA 10-461).

Singh, P., 2008, Lithofacies and sequence stratigraphic framework of the Barnett Shale, northeast Texas: Ph.D. dissertation, University of Oklahoma, 199 p.

Slatt, R. M., and Y. Abousleiman, 2011, Merging sequence stratigraphy and geomechanics for unconventional gas shales: The Leading Edge, p. 274-282.

Slatt, R. M., and N.R. O'Brien, 2011, Pore Types in the Barnett and Woodford gas shales: Contribution to understanding gas storage and migration pathways in fine-grained rocks: AAPG Bulletin, v.95, no.12, p. 2017-2030.

Slatt, R. M., N. Buckner, Y. Abousleiman, R. Sierra, P. Philp, A. Miceli-Romero, R. Portas, N.O'Brien, M. Tran, R. Davis, and T. Wawrzyniec, 2012, Outcrop/behind outcrop (quarry), multiscale characterization of the Woodford Gas Shale, Oklahoma, *in* J. Breyer, eds., Shale reservoirs—Giant resources for the 21st century: AAPG Memoir 97, p. 382-402.

Sloss, L.L., 1963, Sequences in the cratonic interior of North America: Geological Society of America Bulletin, v.74, p. 93-114

Smith, N.D., and R.S. Saunders, 1970, Paleoenvironments and their control of acritarch distribution: Silurian of east-central Pennsylvania: Journal of Sedimentary Petrology, v. 40, p. 324-333.

Strother, P. K., 1996, Acritarchs, *in* J. Jansonius and D. C. McGregor, eds., Palynology: Principles and Applications. Volume I. Principles: American Association of Stratigraphic Palynologists Foundation, Dallas, p. 81-106.

Sullivan, K. L., 1985, Organic facies variation of the Woodford Shale in western Oklahoma: Shale Shaker, v. 35, p. 76–89.

Suneson, N. H., C. Ibrahim., K. Dennis., S. Roberts., T. Michael., R. M. Slatt, and C. G. Stone, 2005, Stratigraphic and structural evolution of the Ouachita Mountains and Arkoma Basin, southeastern Oklahoma and west-central Arkansas: applications to petroleum exploration: Oklahoma Geological Survey Guidebook 34, 128 p.

Suneson, N. H., C. Ibrahim, and R. M. Slatt, 2009, Stratigraphic and structural evolution of the Ouachita Mountains and Arkoma Basin, southeastern Oklahoma and west-central Arkansas: Application to petroleum exploration: 2004 field symposium: Technical Papers, 163 p, 2 plates.

Suneson, N. H., 2010, Petrified wood in Oklahoma: Shale Shaker, v. 60, no. 6, p. 259-273.

Sutherland, P. K., 1988, late Mississippian and Pennsylvanian Depositional History in the Arkoma Basin Area, Oklahoma and Arkansas: Geological Society of America Bulletin, v. 100, p. 1787-1802.

Tappan, H., 1980, The paleobiology of plant protists: W.H. Freeman & Co., San Francisco, 1028 p.

Tran, M. H., S. Chen, R. Sierra, Y. Abousleiman, and R. M. Slatt, 2012, A Geomechanics Approach to Evaluate Gas Shale Fracability: A Case Study with the

Woodford Shale. AAPG (American Association of Petroleum Geologists) Annual Convention, 22-25 April, Long Beach, CA. AAPG Search and Discovery Article #90142 < http://www.searchanddiscovery.com/abstracts/html/2012/90142ace/abstracts/tran.htm> (Accessed January 5, 2013)

Urban, J.B., 1960, Microfossils of the Woodford Shale (Devonian) of Oklahoma: unpublished Masther's thesis, University of Oklahoma, Norman, Oklahoma 77 p.

Vail, P. R., Jr. R. M. Mitchum and S. III. Thompson, 1977, Seismic stratigraphy and global changes of sea level, part 3: relative changes of sea level from coastal onlap, *in*: C. E. Payton, eds., Seismic Stratigraphy — Applications to Hydrocarbon Exploration, Memoir v. 26, American Association of Petroleum Geologists, p. 63–81.

Van Wagoner, J.C., R.M. Mitchum, K.M. Campion, and V.D. Rahmanian, 1990, Siliciclastic sequence stratigraphy in well logs, cores and outcrops: concepts for high resolution correlation of time and facies: AAPG Methods in Exploration Series, no.7, 53 p.

Veeken, P.C.H., 2007, "Seismic stratigraphy, basin analysis and reservoir characterization": Handbook of Geophysical Exploration: Seismic Exploration, 3, Amsterdam, the Netherlands, 509 p.

Vigran, J., O. Mørk, A. Arne, W. Forsberg, W. M. Hermann, and W. Wolfgang, 2008, Tasmanites algae—contributors to the Middle Triassic hydrocarbon source rocks of Svalbard and the Barents Shelf: Polar Research v. 27, p. 360–371.

Von Almen, W.F. 1970, Palynomorphs of the Woodford Shale of south-central Oklahoma with observations on their significance in zonation and paleoecology: Michigan State University, unpublished Ph.D. dissertation, 179 p.

Walliser, O. H., 1996, Global events in the Devonian and Carboniferous, *in* O.H. Walliser, eds., Global Events and Event Stratigraphy: Springer-Verlag, Berlin, p. 225–250.

Wang F.P., and J. F. W. Gale, 2009, Screening criteria for shale gas systems: Gulf Coast Association of Geological Societies Transactions, v. 59, p. 779-793.

Witzke, B. J., 1987, Models for circulation patterns in epicontinental seas applied to Paleozoic faces of North American craton: Palaeoceanography, v. 2, p. 229-248.

Appendix

Appendix 1. Palynological assemblages counts (Digital File)

Appendix 2. Wyche-1 detailed core description (Digital File)